Short title: Screen for suppressors of L*er*/Kas2 incompatibility

NLR mutations suppressing immune hybrid incompatibility and their effects on disease resistance

Kostadin E. Atanasov[1], Changxin Liu[1], Alexander Erban[2], Joachim Kopka[2], Jane E. Parker[3] and Rubén Alcázar[1]

[1] Department of Biology, Healthcare and Environment. Section of Plant Physiology. Faculty of Pharmacy and Food Sciences. University of Barcelona. Spain
[2] Max Planck Institute for Molecular Plant Physiology. Germany.
[3] Department of Plant-Microbe Interactions. Max Planck Institute for Plant Breeding Research. Germany.

List of author contributions

K.E.A., J.K, J.E.P and R.A. designed the research; K.E.A. and R.A. performed research with contributions from C.L. and A.E.; K.E.A., A.E, J.K., J.E.P. and R.A. analyzed data; R.A. conceived the project and wrote the paper with contributions from all authors.

Funding information

This work has been supported by the Ramón y Cajal Program (RYC-2011-07847) of the Ministerio de Ciencia e Innovación (Spain), the BFU2013-41337-P and BFU2017-87742-R grants of the Programa Estatal de Fomento de la Investigación Científica y Técnica de Excelencia (Ministerio de Economía y Competitividad, Spain) co-financed with FEDER (Fondo Europeo de Desarrollo Regional), and the Marie Curie Career Integration Grant (DISEASENVIRON, PCIG10-GA-2011-303568) of the European Union. K.E.A, C.L. and R.A. are members of the Grup de Recerca Consolidat 2017 SGR-604 of the Generalitat de Catalunya. K.E.A. acknowledges support from the Subprograma Estatal de Formación del Ministerio de Economía y Competitividad (BES-2014-068041). R.A. and J.E.P. acknowledge support of Deutsche Forschungsgemeinschaft CRC 680 for part of this work.

Author for correspondence: Rubén Alcázar (ralcazar@ub.edu)

One sentence summary: A suppressor screen for immune-related hybrid incompatibilities identifies multiple *TNL* intragenic mutations improving fitness, with no costs on disease resistance to a local *H. arabidopsidis* isolate.

Abstract

Genetic divergence between populations can lead to reproductive isolation. Hybrid incompatibilities (HI) represent intermediate points along a continuum towards speciation. In plants, genetic variation in disease resistance (*R*) genes underlies several cases of HI. The progeny of a cross between Arabidopsis (*Arabidopsis thaliana*) accessions Landsberg (L*er*, Poland) and Kashmir-2 (Kas-2, central Asia) exhibits immune-related HI. This incompatibility is due to a genetic interaction between a cluster of eight *TNL (TOLL/INTERLEUKIN1 RECEPTOR- NUCLEOTIDE BINDING - LEUCINE RICH REPEAT*) *RPP1* (*RECOGNITION OF PERONOSPORA PARASITICA 1)- like* genes (*R1- R8*) from L*er* and central Asian alleles of a *Strubbelig*-family receptor-like kinase (*SRF3*) from Kas-2. In characterizing mutants altered in L*er*/Kas-2 HI, we mapped multiple mutations to the *RPP1*-like L*er* locus. Analysis of these *suppressor of Ler/Kas-2 incompatibility* (*sulki*) mutants reveals complex, additive and epistatic interactions underlying *RPP1-like* L*er* locus activity. The effects of these mutations were measured on basal defense, global gene expression, primary metabolism, and disease resistance to a local *Hyaloperonospora arabidopsidis* isolate (*Hpa* Gw) collected from Gorzów (Gw), where the Landsberg accession originated. Gene expression sectors and metabolic hallmarks identified for HI are both dependent and independent of *RPP1-like* L*er* members. We establish that mutations suppressing immune-related L*er*/Kas-2 HI do not compromise resistance to *Hpa* Gw. QTL mapping analysis of *Hpa* Gw resistance point to *RPP7* as the causal locus. This work provides insight into the complex genetic architecture of the *RPP1-like* L*er* locus and immune-related HI in *Arabidopsis* and into the contributions of *RPP1-like* genes to HI and defense.

INTRODUCTION

Hybrid vigor is a common phenomenon in plants. Genetic differentiation between individuals of the same species at specific loci can also lead to a dramatic reduction of hybrid fitness in the F_1 or later generations, due to negative epistasis. Certain interacting alleles are not deleterious in their respective backgrounds, but they can become lethal when combined in the same hybrid genome. Such negative genetic interactions might constitute an early stage of species isolation (Coyne, 1992; Coyne and Orr, 2004). Plant hybrid necrosis or hybrid weakness has been documented in crops and model species (Bomblies and Weigel, 2007). In the last decade, identification of genetic determinants of some hybrid incompatibilities (HI) revealed that immune gene variability could underlie this phenomenon. Immune-related incompatible hybrids are temperature-dependent and exhibit reduced growth, deregulated cell death, and sterility (Bomblies et al., 2007; Alcázar et al., 2009; Jeuken et al., 2009; Yamamoto et al., 2010; Chen et al., 2014). The metabolic costs of maintaining a constitutively active immune system might contribute to reduced fitness. In many cases, mapping of causal genes identified at least one polymorphic *Nucleotide-binding/leucine-rich-repeat* (*NLR*) locus encoding intracellular pathogen recognition (NLR) receptors (Alcázar et al., 2012; Chae et al., 2014). *NLR*-interacting loci include other disease *Resistance* (*R*) genes or genes with diverse functions (Bomblies and Weigel, 2007; Alcázar et al., 2009; Yamamoto et al., 2010; Chae et al., 2014). In Arabidopsis (*Arabidopsis thaliana*), the *DANGEROUS MIX 2* (*DM2*) locus mapping to a polymorphic *RPP1* (*RECOGNITION OF PERONOSPORA PARASITICA 1*) - *like* gene cluster underlies at least five documented cases of immune-related HI between accessions Uk-1 (*DM2*, *RPP1-like*) / Uk-3 (*DANGEROUS MIX1*, *SUPPRESSOR OF SALICYLIC ACID INSENSITIVE 4*) (Bomblies et al., 2007), Landsberg *erecta* (L*er*) (DM2, *RPP1-like*) / Kas-2 (*STRUBBELIG RECEPTOR FAMILY 3*) (Alcázar et al., 2009), Bla-1 (*DM2*, *RPP1-like*) / Hh-0 (*DANGEROUS MIX 3*, prolyl aminopeptidase *At3g61540*), Dog-4 (*DM2*, *RPP1-like*) / ICE163 (*DANGEROUS MIX 5*), and TueWa1-2 (*RPP1-like*) /ICE163 (*DANGEROUS MIX 4*, overlapping with *RPP8*) (Chae et al., 2014). Therefore, the *RPP1-like* locus is a hotspot for temperature-dependent immune-related HI in *Arabidopsis* (Alcázar et al., 2009; Chae et al., 2014; Stuttmann et al., 2016).

Immune-related HIs have also been reported in rice, lettuce, tomato, the genus *Capsella*, and other species. An interspecific hybrid weakness in rice involves two dominant loci and three genes (Chen et al., 2014). One locus (*HYBRID WEAKNESS I1*, *HWI1*) contains two *LRR RECEPTOR-LIKE KINASE* genes, both required for incompatibility with the *HWI2* locus, which maps to a *SUBTILISIN-LIKE PROTEASE* gene (Chen et al., 2014). Also in rice, a two-way recessive interaction causing hybrid breakdown involves the *CASEIN KINASE I* (*CKI1*)

gene and an *NLR* cluster (Yamamoto et al., 2010). In lettuce, temperature-dependent hybrid necrosis in an interspecific cross involves two loci, one of them mapping to *RIN4* (*RPM1 INTERACTING PROTEIN 4*), encoding an acylated plasma membrane-associated protein which is a negative regulator of basal anti-microbial defense targeted by different *Pseudomonas syringae* effectors (Jeuken et al., 2009; Khan et al., 2016). In tomato, HI was observed in an interspecific cross involving allelic variants at *Rcr3* and *Cf-2* loci, the latter conferring resistance to the fungus *Cladosporium fulvum* (Krüger et al., 2002). In the genus *Capsella*, HI has been described between *C. grandiflora* and *C. rubella* involving a two-way epistatic interaction between *NPR1* and *RPP5* loci (Sicard et al. 2015). The Dobzhansky-Muller model on genetic incompatibilities is agnostic on whether causal genes diverge into incompatible alleles by drift or selection (Coyne and Orr, 2004). The frequency of immune receptor genes underlying HI is likely a consequence of their rapid evolution in response to pathogen infection pressure (Chae et al, 2014).

The majority of plant disease *R* genes encode NLR proteins. These are classified into two main groups: TNLs (TIR-NLRs) and CNLs (CC-NLRs), based on the presence of a Toll/Interleukin-1 Receptor (TIR) or a coiled-coil CC domain at their N-terminus (Sukarta et al., 2016). *R* genes often reside in clusters and exhibit high polymorphism and copy number variation, through illegitimate recombination, duplication, and gene conversion events (Hurwitz et al., 2010; McHale et al., 2012; Muñoz-Amatriaín et al., 2013). Indeed, together with *RECEPTOR-LIKE KINASE* genes, *NLRs* exhibit signatures of rapid expansion and diversification (Cao et al., 2011; Xu et al., 2011). The *RPP1-like* locus contains a variable number of *TNL* genes in different Arabidopsis accessions, from two in Col-0 to four in Ws-2 (Botella et al., 1998), five to six in Zdr-1 and Est-1 (Goritschnig et al., 2016), and eight in L*er*, Uk-1, and Bla-1 (Alcázar et al., 2009; Chae et al., 2014). *RPP* genes recognize the obligate biotrophic oomycete pathogen, *Hyaloperonospora arabidopsidis* (*Hpa*, formerly *Peronospora parasitica*), which causes downy mildew disease (Botella et al., 1998; Coates and Beynon, 2010). As a naturally co-evolving host-pathogen system, different *Hpa* isolates have been identified that elicit accession-specific resistance responses due to the recognition of different avirulence gene products/effectors (*Arabidopsis thaliana* Recognized, ATR), or effector variants. The *RPP1* resistance locus in Ws-2 and Nd-1 contains *RPP1* genes that exhibit partially overlapping recognition of *Hpa* isolates (Botella et al., 1998; Rehmany et al., 2005). Using an F_2 mapping population derived from a cross between *Hpa* isolates Emoy2 (avirulent) and Maks9 (virulent), $ATR1^{NdWsB}$ was found to be recognized by RPP1-NdA (Rehmany et al., 2005). Genetic variation at *ATR1* conditions *Hpa* recognition by different *RPP1* genes, e.g., *RPP1*-WsB, *RPP1*-NdA, *RPP1*-EstA, and *RPP1*-ZdrA (Rehmany et al., 2005; Sohn et al., 2007; Goritschnig et al., 2016). RPP1 receptors likely also perceive other *ATR* gene products (Botella et al., 1998; Rehmany et al.,

2005). An intriguing question is whether *RPP1* genes involved in immune-related HI provide disease resistance to locally adapted *Hpa* isolates, or their activities in pathogen resistance and incompatibility can be separated.

Here we determine the contribution of different *RPP1-like* genes to L*er*/Kas-2 HI and resistance to a local *Hpa* isolate collected in Gorzów Wielkopolski (Poland), where Landsberg was collected in 1939. In this population, 30% of genetically differentiated Gorzów (Gw) individuals contain a conserved *RPP1-like* L*er* haplotype. This derived haplotype increased in frequency and has been maintained locally for many generations (Alcázar et al., 2014). Through EMS mutagenesis, we identify multiple *suppressors of Ler/Kas-2 incompatibility* (*sulki*) mutants which map to *RPP1-like* L*er R3* and *R8* genes. Generation of CRISPR/Cas9 *RPP1-like* L*er R2*, *R3*, *R4*, and *R8* loss-of-function mutants in a L*er*/Kas-2 NIL background reveals that additive and epistatic interactions between *RPP1-like* gene members contribute to immune-related HI. Global gene expression and metabolite profiling of L*er*/Kas-2 incompatible hybrids and *sulki* suppressors identify metabolic and expression hallmarks for immune-related HI, which are *RPP1-like R8* dependent or independent. Through QTL mapping, we find that resistance to the local *Hpa* isolate from Gorzów (denoted here *Hpa* Gw) in L*er* is not mediated by genes at the *RPP1-like* locus, but maps to a region containing the previously defined *RPP7* CNL *Resistance* gene (McDowell et al., 2000). Resistance conferred by *RPP7* to *Hpa* Gw is genetically independent of salicylic acid (SA) and *EDS1*. Because certain *RPP1-like* proteins recognize allelic variants of the *Hpa* ATR1 effector, we tested whether RPP1-like L*er* proteins could induce host cell death, reflecting a hypersensitive response (HR) when transiently expressed with *Hpa* Gw ATR1 in *Nicotiana tabacum*. Co-expression of *RPP1-like* L*er* R2, R3, R4 or R8 protein with *Hpa* Gw ATR1δ51 does not trigger cell death in *Nicotiana tabacum*. Our results show that the *RPP1-like* incompatible haplotype does not provide disease resistance to a local *Hpa* Gw isolate. We provide evidence for complex genetic interactions underlying the *RPP1-like* L*er* locus HI with Kas-2. Our results also help differentiate *RPP1-like* gene actions in incompatibility and defense.

RESULTS

Identification of *RPP1-like* L*er* suppressors of Ler/Kas-2 incompatibility

An incompatible L*er*/Kas-2 near-isogenic line (NIL) that contains a L*er* introgression spanning the *RPP1-like* locus, in an otherwise Kas-2 genetic background (Alcázar et al., 2009), was used for the isolation of *suppressor of Ler/Kas-2 incompatibility* (*sulki*) mutants. Mutagenized L*er*/Kas-2 NIL plants were generated by treating L*er*/Kas-2 NIL seeds with ethyl methanesulfonate (EMS), and 25,000 M_1 individuals were propagated in 200 pools. Approximately 1,000 M_2 generation plants from each pool were grown to identify suppressors of HI at 14 - 16ºC. Twenty dominant *sulki* mutants were isolated which suppressed dwarfism at 14 - 16ºC, indicative of a loss or amelioration of L*er*/Kas-2 HI. The different *sulki* mutants were backcrossed at least five times with the parental L*er*/Kas-2 NIL. The genomes of *sulki* BC_5F_1 and L*er*/Kas-2 NIL were then sequenced by next-generation sequencing and unique SNPs identified for each mutant compared with the L*er*/Kas-2 NIL.

DNA sequence analysis identified eleven *sulki* mutants carrying single mutations within the *RPP1-like* L*er* locus, which were further confirmed by SANGER sequencing (**Fig. 1A**). Ten intragenic mutations (*sulki1-1* to *sulki1-10*) were dominant, mapping to different domains of *RPP1-like* L*er R8*, and fully suppressed both dwarfism and cell death at low temperature (14 - 16ºC) (**Fig. 1A, Fig. 2, Supplemental Fig. 1 and Supplemental Table 1**). *RPP1-like* L*er R8* is a homolog of *DANGEROUS MIX 2h* (*DM2h*) in Arabidopsis accessions Uk-1 and Bla-1 (Chae et al., 2014). In Col-0, it is homologous to *At3g44670* (Alcázar et al., 2014), although with a high level of polymorphism especially in the LRR domain (Chae et al., 2014). A recessive mutation (*sulki2-1*) mapped to the TIR domain of *RPP1-like* L*er R3* (T78I), which partially suppressed dwarfism and cell death (**Fig. 2, Supplemental Fig. 1 and Supplemental Table 1**). In all cases, except for one 8-nucleotide deletion (*sulki1-7*), only G/C to A/T transition mutations were observed, as expected for mutations generated by EMS treatment (**Fig. 1A**).

Distribution of *sulki* mutations within TIR, NB, and LRR domains

In *RPP1-like* L*er R8*, five and three suppressor mutations were found in the NB and LRR domains, respectively (**Fig. 1B**), consistent with the importance of these domains in TNL function (Meyers et al., 2003). Amino acid changes were found within the conserved RNBS-C (P428S, *sulki1-2*) and GLPL (P466L, *sulki1-3*) motifs. Two additional amino acid substitutions (G500E in *sulki1-5* and G509A in *sulki1-6*), and one stop codon (W484*, *sulki1-4*) were in a stretch of 40 amino acids that connects GLPL and RNBS-D motifs. The presence of three close mutations leading to the same suppressive phenotype suggests that the GLPL-to-RNBS-D region is crucial for *RPP1-like* L*er* R8 function. Three additional amino acid changes were

found in the LRR domain of *RPP1-like* L*er R8*, in the junction between LRR2 and LRR3 (S758F, *sulki1-8*), within LRR5 (R821H, *sulki1-9*) and LRR8 (G877E, *sulki1-10*) motifs. A small 8-nucleotide deletion was identified in the splice donor site of *sulki1-7*, preceding the LRR exon. In the TIR domain of *RPP1-like* L*er R8*, one G202E non-synonymous substitution was detected between TIR3 and TIR4 in *sulki1-1* (**Fig. 1B**). Most suppressive non-synonymous substitutions were found in invariant or highly conserved NLR residues, except for Gly^{509}, which appears to be specific to *RPP1-like* L*er* R8 homologs *At3g44670* $^{Col-0}$ and *DM2h* $^{Bla-1}$ (**Supplemental Fig. 2**).

Altogether, we identified multiple independent mutations within the NB or LRR domains of *RPP1-like* L*er R8* and single mutations in the TIR domains of *RPP1-like* L*er R8* and *R3* genes suppressing L*er*/Kas-2 NIL immune-related HI. These data strongly reinforce previous studies identifying *RPP1-like* L*er R3* and *R8* as genes contributing to L*er*/Kas-2 HI (Alcázar et al., 2014; Stuttmann et al., 2016). We concluded that single point mutations within the *RPP1-like* locus are sufficient for full (*sulki1*, *RPP1-like* L*er R8*) or partial (*sulki2*, *RPP1-like* L*er R3*) suppression of L*er*/Kas-2 HI.

Expression of SA-responsive and oxidative stress marker genes in *sulki1* and *sulki2*

L*er*/Kas-2 HI is associated with constitutive activation of TNL receptor-triggered defense programs, including high expression of *PR1*, *EDS1*, *GST1*, and *RPP1-like* L*er R3* at 14 - 16ºC (Alcázar et al., 2009; Alcázar et al., 2014). We analyzed transcripts of these and other *RPP1-like* L*er* genes (*R2*, *R4*, and *R8*) to determine the defense status of *sulki1* and *sulki2*. Expression of *PR1*, *EDS1*, and *GST1* was much lower in *sulki1* and *sulki2-1* mutants compared to the L*er*/Kas-2 NIL, but similar or slightly lower than L*er* or Kas-2 (**Fig. 3**). These results suggest that constitutive activation of defenses in the L*er*/Kas-2 NIL at 14 - 16ºC is suppressed in *sulki1* and *sulki2*. The expression of *RPP1-like* L*er R3* and *R8* was also significantly lower in *sulki1* and *sulki2* than in L*er*/Kas-2 NIL (**Fig. 3**). We hypothesized that SA, which accumulates in L*er*/Kas-2 NIL (Alcázar et al. 2009), causes up-regulation of some *RPP1-like* genes. Indeed, we found that *RPP1-like* L*er R3* and *R8* but not *R2* or *R4* expression was induced in L*er* by SA or BTH (benzo (1,2,3) thiadiazole-7-carbothioic acid *S*-methyl ester) application at 8 to 24 h (**Supplemental Fig. 3**). Therefore, we concluded that there is SA positive feedback regulation of *RPP1-like* L*er* genes *R3* and *R8* involved in immune-related HI.

Allelism and complementation tests of *sulki1 and sulki2* mutants

To confirm that the causal mutations in *sulki1* map to *RPP1-like* L*er R8*, we performed allelism tests with *RPP1-like* L*er R8* loss-of-function mutants generated by CRISPR/Cas9 in the

L*er*/Kas-2 NIL background (referred to as Cas9-*r8*, **Supplemental Fig. 4**). Cas9-*r8* mutants that contained early stop codons in the TIR domain of *RPP1-like* L*er R8* suppressed dwarfism and cell death at 14 - 16ºC in a dominant manner, consistent with the involvement of *RPP1-like* L*er R8* in the incompatibility with Kas-2 (**Fig. 4A, Supplemental Fig. 5, and Supplemental Table 1**). To confirm that *sulki1* mutations were allelic to Cas9-*r8*, homozygous *sulki1* and Cas9-*r8-1* (after removal of the *Cas9* transgene) were crossed, and F_2 populations were obtained by selfing. The F_2 populations were screened for the occurrence of incompatible phenotypes at 14 - 16ºC (**Supplemental Table 1**). The absence of segregation for incompatibility confirmed that *sulki1* mutants are allelic to Cas9-*r8*.

To confirm the causality of the *sulki2-1* mutation mapping to *RPP1-like* L*er R3*, we transformed *sulki2-1* plants with a genomic construct of *RPP1-like* L*er R3* (Alcázar et al., 2014). Complemented lines, which also were non-overexpressors of the *RPP1-like R3* L*er* transgene, reconstituted the incompatible phenotype at 14 - 16ºC (**Supplemental Fig. 6**). These results are in agreement with a gene dosage effect underlying the recessive nature of the *RPP1-like* L*er* locus. In summary, we confirmed that mutations underlying *sulki1* and *sulki2*-1 suppressive phenotypes map to *RPP1-like* L*er R8* and *R3* genes, respectively.

Generation of *RPP1-like* L*er* loss-of-function mutants in L*er*/Kas-2 NIL by CRISPR/Cas9

We next analyzed the contribution of other *RPP1-like* L*er* genes to L*er*/Kas-2 immune-related HI by isolating CRISPR/Cas9-induced mutations in the L*er*/Kas-2 NIL. Based on mRNA-seq data (see below), *RPP1-like* L*er R2*, *R3*, *R4*, and *R8* genes within the *RPP1-like* L*er* locus are predicted to encode full-length TNL proteins. *RPP1-like* L*er R1*, *R5*, *R6* or *R7* genes contain stop codons in their TIR or NB domains. Therefore, we focused on *RPP1-like* L*er R2*, *R3*, *R4*, and *R8* to introduce frameshift mutations by CRISPR/Cas9 in TIR or NB domains. For each TNL-encoding gene, we designed protospacers next to unique NGG motifs (protospacer adjacent motif, PAM) (Fauser et al., 2014) (**Supplemental Fig. 4**). Indel mutations resulting in early stop codons were identified in transgenic lines expressing specific *RPP1-like* L*er R2*, *R3*, *R4*, and *R8* RNA-guided endonucleases (**Supplemental Fig. 4**). The different mutants were then crossed with L*er*/Kas-2 NIL and Cas9-free homozygous mutants isolated from the F_2 progeny. To confirm the absence of mutations in other genes within the *RPP1-like* cluster, the eight *RPP1-like* L*er* genes were sequenced in the different CRISPR/Cas9 mutants (Alcázar et al., 2014).

Loss-of-function mutations at *RPP1-like* L*er R2* (Cas9-*r2-1* and *r2-2*), *R3* (Cas9-*r3-1* and *r3-2*), and *R4* (Cas9-*r4-1* and *r4-2*) in the L*er*/Kas-2 NIL were recessive and resulted in partial suppression of dwarfism and cell death (**Fig. 4A, Supplemental Fig. 5, and Supplemental**

Table 1). Lower expression of *PR1*, *EDS1*, *GST1*, and *RPP1-like* L*er R3* in 5-week-old Cas9 lines grown at 14 - 16ºC was consistent with suppression of the autoimmune response (**Fig. 4B**). Notably, cell death (**Supplemental Fig. 5C**) and *PR1*, *EDS1*, *GST1*, and *RPP1-like* L*er R3* expression (**Supplemental Fig. 7**) increased over time in Cas9-*r2*, -*r3* and -*r4* lines, although to a lower extent than in the L*er*/Kas-2 NIL. Mutations in *RPP1-like* L*er R8* alone fully suppress incompatibility, regardless of other incompatible genes contributing to HI being present (*RPP1-like* L*er R2*, *R3*, and *R4*). Therefore, incompatibility is not simply an additive effect of various *RPP1-like* L*er* genes with *R8* having stronger effects than the others. These results indicate that *RPP1-like* L*er R2*, *R3*, and *R4* genes contribute additively to L*er*/Kas-2 HI, whereas *RPP1-like* L*er R8* is epistatic to other *RPP1-like* L*er* members. Thus, additive and epistatic interactions underlie the complex nature of *RPP1-like* L*er* cluster incompatibility with Kas-2. The data are consistent with the involvement of two or more *RPP1-like* L*er* genes in HI between L*er* and Kas-2 (Alcázar et al., 2014; Stuttmann et al, 2016).

Bacterial pathogen resistance phenotypes in *sulki1, sulki2,* and Cas9 *RPP1-like* L*er* mutants

We determined the effect of *sulki1*, *sulki2*, Cas9-*r2*, Cas9-*r3*, Cas9-*r4*, and Cas9-*r8* mutations on basal disease resistance by measuring the growth of virulent *Pseudomonas syringae* pv. *tomato* strain DC3000 (*Pst* DC3000) and the Type III secretion-disabled *Pst hrcC* mutant, which fails to deliver virulence factors (effectors) and induces only PAMP-triggered immunity (PTI) (Yuan and He, 1996). At 14 - 16ºC and 20 - 22 ºC, the L*er*/Kas-2 NIL exhibited higher basal resistance to *Pst* DC3000 than all other tested genotypes (**Fig. 5**). At both temperatures, *sulki1* and Cas9-*r8* mutations suppressed L*er*/Kas-2 basal resistance to similar levels as the parents (L*er* or Kas-2). By contrast, *sulki2-1*, Cas9-*r2*, Cas9-*r3*, and Cas9-*r4* mutations exhibited partial suppression of basal resistance at 14 - 16ºC, but full suppression at 20 - 22 ºC (similar to L*er* and Kas-2). These results show that *RPP1-like* L*er R8* mutations in *sulki1* and Cas9-*r8* suppress L*er*/Kas-2 NIL defenses at both temperatures. A suppressive effect was observed in Cas9-*r2*, Cas9-*r3*, and Cas9-*r4* mutants only at 20 - 22 ºC, consistent with their partial suppression of immune-related HI. No differences were detected between lines in response to *Pst hrcC* at either temperature (**Fig. 5**). Notably, mutation in *RPP1-like* L*er R8* did not lead to full susceptibility of the *eds1-2* mutant at both temperatures (**Fig. 5**). From these results, we concluded that suppression of *RPP1-like* L*er R8* function does not lead to a general dampening of basal defenses against *Pst* bacteria.

Gene expression analyses

To determine the effect of *sulki1* mutations suppressing immune-related HI on global expression profiles, we performed RNA-seq analyses in *sulki1-8*, the L*er*/Kas-2 NIL, and Kas-2

plants grown at 14 - 16ºC. A total of 9564 genes exhibited significant expression differences (fold-change ≥ 2; *p*-value and FDR ≤ 0.05) in the comparison between Kas-2 and L*er*/Kas-2 NIL (**Fig. 6 and Supplemental Tables 2-1 and 2-2**). Of these, 5882 genes (61.5 %) were common between *sulki1-8* and L*er*/Kas-2 NIL. Gene ontology analysis of these common genes revealed an enrichment of stress-related terms (**Supplemental Table 2-2**). These genes represent transcriptional responses associated with incompatibility, which are suppressed in *sulki1-8*. However, 3682 other genes were still differentially expressed in the comparison between Kas-2 and L*er*/Kas-2 NIL. These expression changes might be due to differences in the genetic background between Kas-2 and the L*er*/Kas-2 NIL not associated with incompatibility (**Supplemental Table 2-1**). Gene ontology analysis in this subset of genes identified an enrichment of nitrogen metabolism-related terms (**Supplemental Table 2-1**). Finally, RNA-seq analysis identified 622 other genes differentially expressed in *sulki1-8 vs* L*er*/Kas-2 NIL that did not show significant expression differences in Kas-2 *vs* L*er*/Kas-2 NIL. These *sulki1-8*-specific genes were related to oxidation-reduction based on gene ontology (**Supplemental Table 2-3**).

Global metabolite profiling

We determined the effects of *sulki1* mutations on primary metabolism through global metabolite profiling by GC/MS in L*er*/Kas-2 NIL, *sulki1* (*sulki1-1*, *sulki1-7*, *sulki1-8*, and *sulki1-9*) and the parents (L*er* and Kas-2) at 14 - 16ºC. The metabolomics analysis identified 57 metabolites in the analyzed samples, 36 of which were consistently detected in all genotypes and used for principal component analysis (PCA) (**Fig. 7A**). The nature of 23 of these 36 metabolites was known and annotated according to the MPIMP-Golm inventory list (Kopka et al., 2005). Among the identified metabolites, we detected amino acids, polyhydroxy acids, sugars, and TCA cycle intermediates (**Supplemental Table 3**). In the PCA analysis, PC1 explained 50.3% of the total variance and differentiated between the incompatible L*er*/Kas-2 NIL and other genotypes. PC1 indicated that the *sulki1* mutations cause a reversal of a large part of the altered primary metabolome in L*er*/Kas-2 NIL to L*er* or Kas-2 parent levels. This metabolic reversal was consistent with suppression of the dwarf phenotype (**Figure 2**), the absence of cell death at low temperature (**Supplemental Figure 1B**), and deactivation of transcriptional defense responses (**Figure 3**) in the *sulki* mutants. Conversely, PC2 (21.9 % of the total variance) revealed that some metabolic differences remained between *sulki1* mutants or L*er*/Kas-2 NIL and the parents (**Fig. 7A and Supplemental Table 4**).

Hierarchical cluster analysis (HCA) with Pearson's correlation and average linkage of metabolites and genotypes identified metabolic differences between the strongly deviating

L*er*/Kas-2 NIL, the parents, and the *sulki1* mutants (**Fig. 7B**). The heat map representation indicated a large cluster of metabolites that differentially accumulated in L*er*/Kas-2 NIL (**Fig. 7B**). Compared with L*er* and Kas-2, the incompatible L*er*/Kas-2 NIL accumulated amino acids, such as glutamine/pyroglutamate, aspartate, threonine, or alanine, lipid-related phosphate, glycerol, ethanolamine, carbohydrate metabolism related glyceric acid, glucose-6P, and sucrose (**Fig. 7C**). The levels of ascorbate, a substrate of the glutathione-ascorbate cycle for hydrogen peroxide detoxification, were much lower in L*er*/Kas-2 NIL than in the isogenic Kas-2, consistent with the occurrence of oxidative stress induced by HI. On the other hand, dehydroascorbate levels were similar in the two genotypes. These metabolic changes appear to be associated with HI, specifically with growth reduction in combination with metabolic recycling caused by the increased frequency of cell death in L*er*/Kas-2 NIL leaf tissue.

As expected, most metabolic reprogramming associated with HI was reverted in *sulki1* mutants to Kas-2 levels, *e.g.*, ascorbate, sucrose, phosphate, glycerol, aspartate, glutamine/pyroglutamate, and threonine (**Fig. 7C**). However, *sulki1* mutants exhibited metabolic changes that differed from L*er*/Kas-2 NIL, L*er* or Kas-2 (**Fig. 7C**). These changes in the *sulki1* mutants might be linked to *RPP1-like* L*er R8*-independent transcriptional defense activation (**Figure 6**). Levels of glutamate, aspartate, threonine, alanine, and dehydroascorbate were lower than in the parents. In parallel, glucose and fructose levels were consistently higher in *sulki1-1*, *sulki1-7*, *sulki1-8*, and *sulki1-9* compared to the parents L*er*, Kas-2, and the incompatible L*er*/Kas-2 NIL. However, such differences were not observed in the levels of sucrose or glucose-6P (**Fig. 7C**). Quantification of starch at the end of the day (light) and before dawn (dark) in the above genotypes indicated the lower capacity of L*er*/Kas-2 NIL to accumulate starch during the day, although its levels were not depleted at dawn (**Supplemental Fig. 8**). Interestingly, the L*er*/Kas-2 NIL also exhibited higher apoplastic invertase activity than L*er*, Kas-2 or *sulki1*, whereas vacuolar invertase was barely affected (**Supplemental Fig. 9**). These results can be explained by the suggested role of cell wall invertase in plant defense (Tauzin and Giardina, 2014). The absence of glucose or fructose accumulation in the L*er*/Kas-2 NIL, despite the presence of high apoplastic invertase activity, suggests the use of carbohydrates in the biosynthesis of secondary metabolites involved in defense or cell wall strengthening. These demands might contribute to the metabolic costs of diverting resources away from growth in the L*er*/Kas-2 NIL.

Altogether, global metabolite profiling confirmed a physiological reversal of the L*er*/Kas-2 HI metabolic phenotype in *sulki1*. It also reinforced *RPP1-like* L*er R8*-independent responses at a metabolic level that were indicated by transcriptome profiling (**Figure 6**). We concluded that the L*er*/Kas-2 incompatible hybrids are growth inhibited, but that this inhibition is likely not due to limited C-, N-, or P-resources.

Characterization of a pathogenic *Hpa* isolate in the *Arabidopsis* Gorzów population

Previously, we collected a population of L*er* relatives (Gw) in Gorzów Wielkopolski (Poland), in which 30% of individuals carried a conserved *RPP1-like* L*er* haplotype (Alcázar et al., 2014). In 2014, we revisited the population site and isolated *Hpa* naturally infecting Gw plants, for which a basic population structure was already established (Alcázar et al., 2014). *Hpa* was found sporulating on cauline leaves of the susceptible genotype Gw-16. We refer to this local oomycete as *Hpa* Gw, which was propagated as a mass conidiospore culture from a single plant. The *Hpa ATR1* gene, encoding an effector recognized by certain *RPP1-like* TNL receptors, was used to establish a phylogenetic relationship between *Hpa* Gw and other known *Hpa* isolates. Sequencing of *ATR1* from *Hpa* Gw did not identify segregating polymorphisms within this population, which would be indicative of mixed *Hpa* populations. *Hpa* Gw was found to be more related to *Hpa* isolate Cala2 and Emwa1 than other *Hpa* isolates (**Supplemental Fig. 10**).

Examination of *Hpa* Gw disease resistance in 40 genetically different *Arabidopsis* Gw lines identified seven genotypes (17.5 %) that were susceptible to *Hpa* Gw (e.g., Gw-16 in **Supplemental Fig. 11; Supplemental Table 5**). The remaining genotypes, as well as L*er*, Col-0, Kas-2, L*er*/Kas-2 NIL, and cNIL (Alcázar et al., 2010) exhibited a hypersensitive response (HR) indicative of resistance to *Hpa* Gw infection and consistent with host *RPP*-mediated pathogen recognition (**Supplemental Fig. 11)**. T-DNA insertion mutants of *RPP1* and *RPP1-like* genes in Col-0 *At3g44400* (N632237 and N518157), *At3g44480* (N599581 and N655327), *At3g44630* (N644159 and N658450), and *At3g44670* (N529707 and N477722) did not support the growth of *Hpa* Gw and exhibited HR (**Supplemental Fig. 11)**. Susceptible and resistant Gw genotypes were not differentiated from each other in PCA analyses based on 134 genome-wide distributed SNP (Alcázar et al., 2014) (**Supplemental Fig. 12**). Notably, however, all genotypes carrying the conserved *RPP1-like* L*er* haplotype were resistant to *Hpa* Gw infection (**Supplemental Fig. 12 and Supplemental Table 5**). Despite this, resistance is not strictly associated with the presence of an *RPP1-like* L*er* haplotype because it is expressed in accessions that do not carry the haplotype (e.g., Col-0).

Effect of suppressive mutations on *Hpa* Gw disease resistance in L*er*/Kas-2 NIL

Next, we studied the effect of the L*er*/Kas-2 HI suppressor (*sulki*) mutations on resistance to the local *Hpa* Gw isolate in the L*er*/Kas-2 NIL. For this, we inoculated Cas9-*r2*, Cas9-*r3*, Cas9-*r4*, Cas9-*r8*, *sulki1* (*sulki1-3*, *sulki1-7*, *sulki1-8, and sulki1-9*), *sulki2-1*, and *nde1-3*, which carries a deletion between *RPP1-like R3-R8* L*er* genes (Stuttmann et al., 2016). Resistance to *Hpa* Gw was observed in all genotypes tested (**Supplemental Fig. 11)**. We concluded that mutations

suppressing L*er*/Kas-2 incompatibility do not compromise disease resistance to a local *Hpa* isolate.

Analysis of ATR1 Gw recognition by RPP1-like L*er* proteins in *N. tabacum*

RPP1-like TNL receptors directly recognizing ATR1 effector variants from different *Hpa* isolates have been characterized (Rehmany et al., 2005; Sohn et al., 2007; Krasileva et al., 2010). We determined the capacity of TNL RPP1-like L*er* R2, R3, R4, and R8 proteins to recognize ATR1 cloned from Gw leading to cell death in *Nicotiana tabacum* transient expression assays. For this, C-terminal YFP fusions of *RPP1-like* L*er R2*, *R3*, *R4*, *R8* genomic constructs, and ATR1-δ51 *Hpa* Gw (lacking the ATR1 secretory signal peptide) (Steinbrenner et al., 2015) were generated for *Agrobacterium tumefaciens* infiltration of tobacco leaves. Accumulation of *RPP1-like* L*er* R3 protein over a threshold triggered cell death in *N. tabacum* leaves (**Fig. 8A**), consistent with L*er*/Kas-2 NIL phenotypes induced by *R3* overexpression in *Arabidopsis* (Alcázar et al., 2014), and its involvement in L*er*/Kas-2 immune-related HI (**Fig. 4**). However, 1:1 co-infiltration of δ51-ATR1 *Hpa* Gw with *RPP1-like* L*er* R2, R3, R4 or R8, which resulted in lower but detectable RPP1 protein expression in *N. tabacum* leaves, did not induce cell death (**Fig. 8B**). These results suggest that ATR1 *Hpa* Gw is not recognized by any of the RPP1-like L*er* variants tested.

***Hpa* Gw disease resistance is independent of *EDS1* and *ICS1*-generated SA**

We tested whether resistance to *Hpa* Gw was compromised in *eds1-2* (Col-0) (Bartsch et al., 2006), *eds1-2* (L*er*) (Feys et al., 2005), the SA-deficient *ISOCHORISMATE SYNTHASE 1 sid2-1* mutant (Col-0) (Wildermuth et al., 2001), or L*er-NahG* transgenic plants that metabolize SA into catechol (Bowling et al., 1994). Neither *eds1-2* nor SA depletion affected resistance to *Hpa* Gw (**Supplemental Fig. 11)**. Because *TNL* immunity relies on *EDS1* (Aarts et al., 1998; Feys et al., 2001; Feys et al., 2005) and the *RPP1-like* L*er* locus only contains *TNL* genes (Alcázar et al., 2009), we reasoned that resistance to *Hpa* Gw is governed by other *RPP* loci in the genome.

Mapping of *Hpa* Gw disease resistance

Whereas L*er* is resistant to *Hpa* Gw, we found that the Shakdara (Sha) accession is susceptible, which enabled us to exploit a L*er*/Sha recombinant inbred line (RIL) population (Clerkx et al., 2004) in QTL mapping of *Hpa* Gw resistance loci (**Supplemental Table 6**). QTL analyses identified one major-effect QTL on chromosome 1 explaining 52% of the phenotypic variation, with L*er* alleles contributing most resistance to isolate *Hpa* Gw. L*er*/Sha RILs carrying Sha alleles at this QTL, but L*er* alleles at the *RPP1-like* locus, were susceptible to *Hpa* Gw infection (**Supplemental Table 6**). Therefore, the *RPP1-like* L*er* locus does not confer resistance to *Hpa* Gw. The QTL spanned 2.83 Mb between markers F6D8-94 and GENEA. This region contains

at least nine *CNL* genes, among them *RPP7* (*At1g58602*, **Supplemental Table 7**), which was reported to confer resistance to *Hpa* isolate Hiks1 in an SA- and *EDS1*- independent manner (McDowell et al., 2000) (**Fig. 9A**). Therefore, we consider *RPP7* as a strong candidate gene in L*er* resistance to *Hpa* Gw.

In addition to QTL analyses, we performed GWAS mapping using 288 Arabidopsis accessions distributed worldwide. Of the total phenotyped accessions, 78 (27%) were susceptible to *Hpa* Gw infection. Disease resistance phenotypes did not follow obvious geographical or population structure patterns, and segregated between and within populations (**Supplemental Table 8**). GWAS analysis for *Hpa* Gw disease resistance identified a significant association with multiple SNP belonging to gene *At3g24580*, encoding an F-box protein of unknown function (**Fig. 9B and Supplemental Table 9**). However, no genetic variation at *At3g24580* was found between *Hpa* Gw resistant (Gw-30, Gw-31, Gw-112, Gw-127 and Gw-144) and susceptible (Gw-16, Gw-50, Gw-107, Gw-148, and Gw-167) genotypes, which all carried *At3g24580* Col-0 alleles (**Supplemental Table 5**). We concluded that *At3g24580* does not condition differences in disease resistance to *Hpa* Gw in the Gorzów population, although its epistatic interaction with other genes cannot be excluded in other genetic backgrounds. Together, the QTL and GWAS mapping identified candidate *RPP* genes outside the *RPP1-like* locus as conferring resistance to *Hpa* Gw.

DISCUSSION

Epistasis, defined as the non-additive interaction between mutations, is the basis for many post-zygotic immune-related HI in plants (Bomblies, 2010). The environment can affect the consequences of epistasis on fitness (Flynn et al., 2013). Indeed, growth defects in L*er*/Kas-2 NIL at 14 - 16ºC are suppressed at 20 - 22 ºC (Alcázar et al., 2009), a temperature at which basal disease resistance to *Pst* DC3000 is retained (**Fig. 5**). HI is not the result of direct action by natural selection but rather a byproduct of divergence through evolutionary processes acting on other traits (Coyne and Orr, 2004). Selective forces acting on *R* genes involve arms races between plants and pathogens, in addition to environmental factors (Dodds and Rathjen, 2010; Ariga et al., 2017). Such divergence might thus be shaped by adaptation to different environments (ecological speciation) or through different pathways within the same environment (Sherlock et al., 2017). Adaptive mutations increasing fitness can be retrieved by experimental evolution, an approach facilitated by the study of microbial populations during multiple generations. In yeast, adaptation to divergent and identical environments has been shown to promote the emergence of reproductive isolation (Dettman et al., 2007; Ono et al.,

2017). However, the intrinsic lethal nature of incompatible hybrids hinders the identification of potential mutations suppressing negative epistasis. Here, we circumvented this limitation by inducing random and CRISPR/Cas9-guided mutagenesis in a large population of L*er*/Kas-2 NIL plants. Through this approach, we identified *RPP1* intragenic mutations that suppress L*er*/Kas-2 immune-related HI and observed different degrees of phenotypic adaptation.

The mutagenesis screen identified a large number of intragenic *suppressors of Ler/Kas-2 incompatibility* (*sulki*) mapping to *RPP1-like* L*er R8* (*sulki1*-1 to *sulki1-10*) and one mutation mapping to *RPP1-like* L*er R3 (sulki2-1)* that suppressed HI (**Fig. 2**). Due to the presence of moderate suppressor phenotypes in the EMS population, we reasoned that intragenic mutations leading to intermediate phenotypes might have been overlooked, including mutations in other potential *RPP1-like R3* alleles. Therefore, to provide a comprehensive analysis of the *RPP1-like* L*er* locus, we mutated each *RPP1-like* L*er* TNL encoding gene by CRISPR/Cas9 in the L*er*/Kas-2 NIL background (Cas9-*r2*, Cas9-*r3*, Cas9-*r4*, and Cas9-*r8*) and studied the effects of the mutations on growth, cell death, gene expression, and disease resistance. EMS and CRISPR/Cas9 mutagenesis revealed epistatic interactions between *RPP1-like* L*er R8* and other *RPP1-like* L*er* members (*R2*, *R3*, and *R4*), with the latter contributing additively to immune-related HI (**Fig. 4**). These results are consistent with the involvement of two or more *RPP1-like* genes in L*er*/Kas-2 incompatibility and suggest co-action between *RPP1-like* members for defense activation in *Arabidopsis* (Alcázar et al., 2014). The dominant nature of *RPP1-like* L*er R8* loss-of-function mutations suggests that a certain dosage of incompatible RPP1-like protein is required for the autoimmunity phenotype, and loss-of-function alleles in *RPP1-like* L*er R8* lower this dosage below a critical level when heterozygous. This might also explain the recessive nature of the *RPP1-like* haplotype in L*er*/Kas-2 immune-related HI (Alcázar et al., 2009; Alcázar et al., 2014).

L*er*/Kas-2 HI suppressor mutations mapped to different domains of *RPP1-like* L*er R8* (**Fig. 1**). The different mutations behaved like Cas9-*r8* loss-of-function alleles, indicating that *sulki1* mutations disrupt *RPP1-like* L*er R8* function in L*er*/Kas-2 HI (**Fig. 4**). RNA-seq analyses in *sulki1-8* show that many transcriptional changes in incompatible L*er*/Kas-2 hybrids are suppressed by *RPP1-like* L*er R8* mutation. However, the expression of other genes related with oxidation-reduction was modified in *sulki1-8* mutants compared to its isogenic Kas-2 genotype (**Fig. 6 and Supplemental Tables 2-1 to 2-3**). The occurrence of these *RPP1-like* L*er R8*-independent expression sectors supports a multigenic basis for the *RPP1-like* L*er* incompatible haplotype. Importantly, such expression sectors alone are not sufficient to trigger incompatibility, which requires a functional R8 protein.

Most *sulki1* suppressor mutations in *RPP1-like* L*er R8* were found in NB or LRR domain conserved motifs and invariable residues. The NB-ARC domain is involved in nucleotide binding and hydrolysis and acts as a molecular switch for NLR activation (van Ooijen et al., 2008; Takken and Goverse, 2012). The NB-ARC is required for RPP1 self-association and cell death activation, probably assisted by TIR-TIR interactions (Schreiber et al., 2016). The LRR domain of TNL proteins is often involved in effector recognition, inducing a conformational change that switches the protein to an active state (van Ooijen et al., 2008; Takken and Goverse, 2012; Steinbrenner et al., 2015). Non-synonymous substitutions in the LRR domain of *DM2h* Bla-1 are responsible for incompatibility with *DM1* Hh-0. Certain ATR1 alleles from *Hpa* isolates are recognized by the LRR domain of *RPP1* Ws-0 and Nd-1 (Krasileva et al., 2010; Steinbrenner et al., 2015). The identification of *DM2h* Bla-1 incompatible-trigger mutations in the *LQQL* motif of LRR4, next to a modeled ATR1 docking site, suggested that incompatible *RPP1* variants originate from an arms race between the immune receptor and pathogen ligands (Chae et al., 2014). Notably, the *sulki1-9* mutation (R821H) in LRR5 of *RPP1-like* R8 L*er* is adjacent to this *LQQL* motif (**Fig. 1**). A frameshift mutation in LRR2 of *RPP1-like* L*er R8* in the *nde1-1* (*near death experience1-1*) mutant also suppresses incompatibility with Kas-2. The *nde1-1* mutant was isolated from a suppressor screen for autoimmune phenotypes associated with EDS1 nuclear enrichment and suggested a role for *RPP1-like* L*er R8* in EDS1/PAD4 defense amplification (Stuttmann et al., 2016). Thus, polymorphism at the LRR domain of *RPP1-like* L*er R8* and its homolog in Bla-1 (*DM2h*) seems to be relevant for incompatibility (Chae et al., 2014; Stuttmann et al., 2016).

Here, we find that mutations in the TIR domains of RPP1-like L*er R3* and *R8* also suppress L*er*/Kas-2 immune-related HI (**Fig. 1**). The TIR domain is necessary for receptor signaling, and in some TNLs, including RPP1, this domain self-associates and is sufficient for triggering cell death (Swiderski et al., 2009; Bernoux et al., 2011; Williams et al., 2014; Steinbrenner et al., 2015; Schreiber et al., 2016; Zhang et al., 2017). Whether *sulki1-1* and *sulki2-1* mutations disrupt potential self-association of *RPP1-like* L*er* R3 or R8 proteins needs to be determined.

We investigated whether the *RPP1* L*er* genes contributing to HI also participate in *Hpa* Gw recognition (Krasileva et al., 2010; Steinbrenner et al., 2015). Our analysis, using a local *Hpa* Gw isolate, indicated that the incompatible *RPP1* L*er* haplotype does not contribute to disease resistance to this local pathogen and that the resistance is SA- and *EDS1*-independent (**Supplemental Fig. 11**). Furthermore, we found that co-expression of *RPP1-like* L*er* R2, R3, R4 or R8 proteins with ATR1-δ51 *Hpa* Gw did not trigger HR in *N. tabacum* transient expression assays (**Fig. 8B**). Moreover, QTL mapping in the L*er*/Sha RIL population identified a major QTL on chromosome 1 that contained L*er* alleles contributing to resistance (**Fig. 9A**).

The QTL interval spanned several *R* genes including *RPP7*, a known *CNL* gene governing resistance to the *Hpa* Hiks1 isolate in an SA- and *EDS1*-independent manner (McDowell et al., 2000) (**Supplemental Table 7**). From these data, we concluded that the incompatible *RPP1-like* L*er* haplotype does not contribute to disease resistance to a local *Hpa* isolate. Also, intragenic mutations suppressing L*er*/Kas-2 incompatibility do not incur on a fitness cost in terms of *Hpa* resistance (**Supplemental Fig. 11**). However, such mutations dampen disease resistance to *Pst* DC3000 of the L*er*/Kas-2 NIL at 20–22 ºC (**Fig. 5**), which might represent a trade-off between growth and basal defenses against virulent leaf-colonizing *Pseudomonas* bacteria.

Hpa populations might have diverged or even been extinguished since the birth of the *RPP1-like* L*er* haplotype, which was already present in the Gorzów population in 1939 (Alcázar et al., 2014). Thus, the contemporary *Hpa* Gw isolate might not represent a selective force for the *RPP1-like* L*er* incompatible haplotype. However, fine-tuning *RPP1-like* L*er R3* expression may benefit disease resistance to other pathogenic strains (Alcázar et al., 2014), thereby favoring selection of the incompatible haplotype. Interestingly, *RPP1-like* L*er R3* and *R4* are homologs of *At3g44400* Col-0 (Alcázar et al., 2014) and whole-genome sequencing revealed the absence of *At3g44400* Col-0 gene in L*er* (**Supplemental Fig. 13**). This suggests that *RPP1-like R3* and *R4* in L*er* are derived from a gene transposition and duplication event from *At3g44400*, during the formation of the incompatible *RPP1-like* haplotype.

Incompatible L*er*/Kas-2 NIL plants exhibit metabolic hallmarks of HI which can be explained by a combination of growth arrest and metabolic recycling of material from dead or dying leaf cells. Recycling likely also involves proteolysis and triglyceride degradation accompanied by oxidative stress (**Fig. 7C**). We further detected a promotion of sucrose degradation through cell wall invertase, but not vacuolar invertase activities (**Supplemental Fig. 9**). Activation of cell wall invertase is triggered by defense responses to various pathogens, including oomycetes and bacteria (Tauzin and Giardina, 2014). Glucose and fructose can be used as carbon sources for the biosynthesis of defense-related metabolites, potentially leading to a metabolic cost that reduces growth in the dwarf L*er*/Kas-2 NIL (Bolton, 2009). Remarkably, these metabolic costs are fully suppressed in *sulki1* mutants, which also suppress oxidative stress symptoms. Nevertheless, *sulki1* mutants accumulate higher levels of glucose, fructose, and starch than the L*er*/Kas-2 NIL (**Fig. 7C**), possibly due to *RPP1-like* L*er R8*-independent transcriptional activation of defense responses.

Our data shed light on the complex genetic nature of the *RPP1-like* L*er* locus triggering incompatibility with Kas-2. Through random and guided mutagenesis, mutations can be

generated that mitigate fitness costs of L*er*/Kas-2 HI, while retaining resistance to a local *Hpa* Gw isolate. However, trade-offs are also inherent to such compensatory mutations.

MATERIALS AND METHODS

Plant material and growth conditions

A complete list of *Arabidopsis thaliana* accessions used in this study is provided in **Supplemental Table 8**. Seeds were obtained from the Notthingham Arabidopsis Stock Center (NASC) or collected by authors (Alcázar et al., 2014). The incompatible L*er*/Kas-2 NIL and cNIL used in this study were described before (Alcázar et al., 2009; Alcázar et al., 2010). Plants were grown on soil at indicated temperatures under 12 h dark /12 h light cycles and 70% relative humidity and 120 µmol m^{-2} s^{-1} of light intensity.

EMS mutagenesis

Seeds of L*er*/Kas-2 NIL were soaked overnight in 1 mg/ml KCl at 4ºC. After seed imbibition, the solution was discarded and replaced with 0.2 % EMS (v/v) and incubated for 16 h. Seeds were then washed ten times with 50 ml of water and suspended in 0.1 % agarose for sowing on soil. Approximately 25,000 M_1 plants were allowed to self at 20 – 22ºC. M_2 seeds were collected in pools of 100 to 150 M_1 plants. M_2 plants were grown at 14 – 16ºC to identify suppressors of L*er*/Kas-2 incompatibility (*sulki*).

Whole genome sequencing

Genomic DNA from *Arabidopsis thaliana* plants was extracted from leaves of 5-week old plants grown on soil using the CTAB method (Doyle, 1991). DNA quality was checked on 0.8 % agarose gel electrophoresis stained with ethidium bromide. DNA concentration was determined by fluorometric quantitation using the dsDNA HS assay kit and the "*Qubit"* device (Thermo Fisher). Whole genome sequencing was performed at the *Centro Nacional de Análisis Genómico* (CNAG, Spain). A standard Illumina protocol was followed to create paired-end libraries, which were run on Illumina sequencers Hiseq3000/4000 2x150 according to standard procedures. Sample statistics are shown in **Supplemental Table 10**. Read mapping and variant detection were performed using the *CLC Genomics Workbench 10 version 10.1.1* (Qiagen).

RT-qPCR expression analyses

Total RNA was extracted using *TRIzol* reagent (Termo Fisher). Reverse transcription and quantitative real-time PCR was performed as described (Alcázar et al., 2014). A complete list of primers used for expression analyses is reported in (Alcázar et al., 2014).

649

650 **RNA-seq expression analyses**

651 Total RNA was extracted from fully expanded leaves of 5-week-old *sulki1-8*, Kas-2, and
652 L*er*/Kas-2 NIL plants grown at 14 - 16ºC. Three biological replicates, each from pooled leaves
653 of at least three independent plants grown in individual pots were used for the analysis. Total
654 RNA was extracted using *TriZol* (Thermo Fisher) and quantified in a *Nanodrop ND-1000*
655 spectrophotometer, and checked for purity and integrity in a *Bioanalyzer-2100* device (Agilent
656 Technologies). RNA samples were further processed by the *Centro Nacional de Análisis*
657 *Genómico* (CNAG, Spain) for library preparation and RNA sequencing. Libraries were prepared
658 using the Illumina *TruSeq Sample Preparation Kit* according to manufacturer's instructions.
659 Each library was paired-end sequenced (2 x 75 bp) on HiSeq2000 Illumina sequencers. Sample
660 statistics are shown in **Supplemental Table 10.** Read mapping and expression analyses were
661 performed using the *CLC Genomics Workbench 10 version 10.1.1* (Qiagen). Only significant
662 expression differences (fold-change ≥ 2; *p*-value and FDR ≤ 0.05) were considered.

663

664 **CRISPR/Cas9 mutagenesis**

665 To identify specific PAM motifs in *RPP1-like* L*er* genes, their sequences were aligned using
666 MUltiple Sequence Comparison by Log-Expectation (MUSCLE,
667 http://www.ebi.ac.uk/Tools/msa/muscle/) and unique NGG motifs identified in TIR or NB
668 domains of *RPP1-like* Ler *R2*, *R3*, *R4*, and *R8*. Generation of CRISPR/Cas9 lines was based on
669 the system reported by (Fauser et al., 2014). Spacers were designed next to unique PAM sites,
670 and annealed oligonucleotides containing *BbsI* sites were used for the generation of customized
671 RNA chimeras in the pEn-Chimera vector (**Supplemental Table 11**). The customized RNA
672 chimeras were transferred into pDe-CAS9 by Gateway LR reaction (ThermoFischer). The final
673 clones were sequenced and transformed into *Agrobacterium tumefaciens* GV3101 pMP90.
674 L*er*/Kas-2 NIL plants were transformed by floral dipping and transgenic lines isolated by
675 selection with 20 µg/ml glufosinate-ammonium (Sigma Aldrich). Individual lines were checked
676 for the presence of indel mutations by SANGER sequencing of all *RPP1-like* L*er* genes
677 (Alcázar et al., 2014), crossed to L*er*/Kas-2 NIL and Cas9-free homozygous mutants isolated in
678 the F_2 by gene sequencing and Cas9 genotyping (**Supplemental Table 11**).

679

680 **Histochemical analyses and determination of leaf area.**

681 Plant cell death and *Hpa* structures were determined by staining leaves with lactophenol trypan
682 blue (Alcázar et al., 2009). Samples were mounted on glycerol 70 % and observed under light
683 microscope (Axioplan, Carl Zeiss) coupled to a Leica DFC490 digital camera. Leaf area was
684 quantified using Image Pro Analyzer (Media Cybernetics, Inc.) as reported in (Alcázar et al,
685 2009).

Isolation of *Hyaloperonospora arabidopsidis* Gw and pathogen inoculation assays.

Original spores from *Hyaloperonospora arabidopsidis* Gw were collected from the Gw-16 accession naturally growing in the Gorzów population during spring of 2014. Spores were resuspended in 100 µl of water and inoculated on the susceptible Ws *eds1-1* genotype (Falk et al., 1999). Thereafter, the *Hpa* Gw isolate has been maintained by weekly propagation on the susceptible Gw-16 accession. *Hpa* inoculation assays were performed as described in (Alcázar et al., 2009). *Pseudomonas syringae* spray-inoculation and growth quantitation assays were performed as described in (Alcázar et al., 2010).

Cloning of *ATR1*

The genomic DNA from *Hpa* Gw mass conidiospores was extracted using TriZol (Thermo Fisher) and used for PCR amplification of *ATR1* gene using primer combinations listed in **Supplemental Table 11** (Rehmany et al., 2005). The PCR product was treated with ExoSap (Thermo Fisher) and sequenced by SANGER with primers described in **Supplemental Table 11**.

Global metabolite profiling

Metabolite profiling was performed from leaf samples (120 mg) using at least 10 biological replicates. Polar primary metabolite extraction and gas chromatography coupled to electron impact ionization-time of flight-mass spectrometry (GC/EI-TOF-MS) analysis was performed as described (Zarza et al., 2017). Only metabolites identified in all genotypes and at least 8 of 10 replicates were considered. Normalized values are referred to the internal standard. Principal component analysis was determined using *R* (www.r-project.org). HCA with Pearson correlation was obtained using the MultiExperiment Viewer software (www.tm4.org/mev; version 27 4.8.1).

Starch quantification

The entire shoot of 5-week-old plants was used for the analyses. Samples were harvested 1 h before the end of the light or dark periods. Starch levels were quantified according to (Smith and Zeeman, 2006) using at least five biological replicates per genotype.

Invertase activities

Cell-wall-bound and soluble acid invertase activities were performed according to (Appeldoorn et al., 1997) from leaves of 5-week-old *Arabidopsis* plants using at least 5 biological replicates per genotype.

Transient expression assays

Genomic versions of *RPP1-like* L*er R2, R3, R4*, and *R8* were obtained by PCR amplification from L*er* gDNA using the primers combinations listed in **Supplemental Table 11**. The PCR products were purified and cloned into the pSPARKII vector (Canvax). The resulting clones were sequenced using primers already described (Alcázar et al., 2014) and subcloned SalI/NotI into a modified version of pENTR1A providing gentamycin resistance. The resulting construct was used for LR Gateway (Thermo Fisher) reaction with pEarley101 (Earley et al., 2006) to generate C-terminus YFP-HA fusions of genomic clones under the control of the CaMV 35s promoter. The different constructs were sequenced, transformed into *Agrobacterium tumefaciens* GV3101 pMP90, and used for infiltration of *Nicotiana tabacum* (Samsun, SNN) leaves. Transformed agrobacteria were inoculated into 30 ml YEB media and incubated shaking at 250 rpm and 28 ºC overnight. Cultures were centrifuged at 4,000 *g* for 5 min and resuspended on 10 mM $MgCl_2$ and 10 mM MES pH 5.6 to an OD600 = 0.45. For induction of agrobacteria virulence, 150 µM acetosyringone was added to the cells for 3 h. Discs from inoculated leaves were collected at indicated time points using a cork borer (1.2 cm diameter) and frozen immediately in liquid nitrogen. Pictures were taken at indicated time points with a Canon EOS 450D digital camera.

Western blot analysis

Frozen samples were disrupted in 1.5 ml tubes along with 1 mm glass beads in a homogenizer device. Samples were suspended on 200 µl of protein extraction buffer (0.24 M Tris pH 6.8, 6 % SDS, 30 % glycerol, 16 % 2-mercaptoethanol, 0.01 % bromophenol blue and 10 M urea), boiled for 5 min and centrifuged for 5 min at 12,000 g. The supernatant was then transferred to a new tube. 15 µl were used for 8 % SDS-PAGE electrophoresis and transferred by blotting to a PVDF membrane. Anti-GFP monoclonal antibody (clones 7.1 and 13.1) (Roche) at 1:1,000 dilution and rabbit-anti-mouse HRP (Sigma Aldrich) secondary antibody at 1:10,000 were used for detection of YFP tagged proteins with SuperSignal West Femto Maximum Sensitivity Chemiluminescent Substrate (Thermo Fisher).

QTL and GWAS mapping

QTL mapping was performed using *R/qtl* with the genetic data of the L*er*/Sha RIL population from (Clerkx et al., 2004) and phenotype evaluation of *Hpa* Gw disease resistance in **Supplemental Table 6**. For phenotypic evaluation, values from 0 to 2 were assigned to each genotype (0, no sporulation; 1, sporulation only observed on cotyledons; 2, sporulation observed in cotyledons and fully expanded leaves). LOD scores were calculated with a single-QTL model implemented in *R/qtl*. LOD score significance threshold was established using 1,000 permutations. GWAS mapping was performed using accessions and phenotypes listed in

Supplemental Table 8. Manhattan plots were determined using 250k SNP data and the accelerated mixed model (*AMM*) (Kang et al., 2010; Zhang et al., 2010) implemented in GWAPP (Seren et al., 2012). To ensure adequate correction for population stratification we constructed a *quantile-quantile* plot (**Supplemental Fig. 14**). A list of most significant associations is found in **Supplemental Table 9**.

Accession numbers

RNA-seq data has been deposited to ArrayExpress (www.ebi.ac.uk/arrayexpress/) under accession number E-MTAB-6755.

Acknowledgments

We thank Maarten Koornneef for biological materials and critical reading of the manuscript.

We acknowledge support from the Centro Nacional de Análisis Genómico (CNAG, Spain) in next-generation sequencing experiments.

FIGURE LEGENDS

Figure 1. *sulki1* mutations mapping to *RPP1-like R8* L*er*. **(A)** Schematic representation of non-synonymous substitutions identified in *sulki1* mutants. Exon/intron organization and Toll-interleukin receptor (TIR), nucleotide binding (NB) and leucine-rich repeat (LRR) domains are shown. **(B)** Detailed representation of *RPP1-like R8* L*er* amino acid sequence, conserved motifs (Meyers et al., 2003) and position of *sulki1* mutations.

Figure 2. Composite image of *sulki* phenotypes. 5-week-old *sulki1*, *sulki2*, L*er*/Kas-2 NIL grown at 14 - 16ºC under 12 h light / 12 h dark cycles and light intensity of 120 µmol/m^2sec.

Figure 3. Expression of SA and oxidative stress marker genes. Quantitative reverse transcription PCR (RT-qPCR) analyses of *PR1*, *EDS1*, *GST1*, *RPP1-like* L*er R2*, *R3*, *R4*, and *R8* genes in *sulki1-1* (*s1-1*) to *sulki 1-10* (*s1-10*), *sulki2-1* (*s2-1*), L*er*, Kas-2, L*er*/Kas-2 NIL and NIL complemented with *SRF3* L*er* (cNIL) (Alcázar et al., 2010). Values are relative to L*er* and are the mean of three biological replicates, each with three technical replicates. Letters indicate values that are significantly different according to Student–Newman–Keuls test at *P* value <0.05. Error bars indicate standard deviation.

Figure 4. Growth phenotypes and expression analyses of Cas9 *RPP1*-like L*er* mutants. **(A)** Composite image of 5-week-old Cas9-*r2-1*, Cas9-*r3-1*, Cas9-*r4-1*, Cas9-*r8-1* mutants in the L*er*/Kas-2 NIL background, L*er*/Kas-2 NIL and parental lines (L*er* and Kas-2) grown at 14 - 16ºC. The position of stop codons in TIR (T) or NB (N) domains of *RPP1-like* genes is marked with an asterisk. **(B)** Gene expression analyses of *PR1*, *EDS1*, *GST1*, *RPP1-like* L*er R2*, *R3*, *R4* and *R8* in Cas9 *r2-1*, *r2-2*, *r3-1*, *r3-2*, *r4-1*, *r4-2*, *r8-1* and *r8-2* mutant alleles, L*er*, Kas-2, L*er*/Kas-2 NIL and cNIL plants grown at 14 - 16ºC during five weeks. Analyses were performed as described in **Fig. 3**.

Figure 5. Growth of *Pseudomonas syringae* pv tomato (*Pst*) DC3000 and *hrcC* mutant, 3 days after spray inoculation of *sulki1-1* (*s1-1*), *sulki1-7* (*s1-7*), *sulki1-8* (*s1-8*), *sulki1-9* (*s1-9*), *sulki2-1* (*s2-1*), Cas9- *r2-1*, *r3-1*, *r4-1* and *r8-1* mutants in the L*er*/Kas-2 NIL background, L*er*, Kas-2, L*er*/Kas-2 NIL and *eds1-2* L*er* plants grown at 20 – 22 ºC **(A)** or 14 – 16ºC **(B)**. Different letters indicate significant differences (P < 0.01) in a Student-Newman Keuls test. Error bars indicate standard deviation.

Figure 6. Venn diagram of genes differentially expressed in the comparisons between (Kas-2 *vs* L*er*/Kas-2 NIL) and (*sulki1-8 vs* L*er*/Kas-2 NIL). Lists of genes and gene ontology analyses are included in **Supplemental Tables 2-1 to 2-3**.

Figure 7. (A) Principal component analysis and **(B)** Hierarchical cluster analysis (*HCA*) with Pearson's correlation and average linkage of samples and metabolites from 5-week-old *sulki1-1* (*s1-1*), *sulki1-7* (*s1-7*), *sulki1-8* (*s1-8*), *sulki1-9* (*s1-9*), L*er*, Kas-2, and Ler/Kas-2 NIL plants grown at 14 -16ºC. **(C)** Log_2-normalized responses for some metabolites determined by GC/MS in the above genotypes, and schematic representation of their metabolic pathways. Different letters indicate significant differences (P < 0.01) in a Student-Newman Keuls test. Error bars bars indicate standard deviation. A complete list of analyzed metabolites is provided in **Supplemental Table 3**.

Figure 8. Transient expression assays in *Nicotiana tabacum*. **(A)** Transient expression of genomic versions of 35s: *RPP1-like* L*er R2*, *R3*, *R4*, *R8*, and ATR1-δ51 Gw, tagged with C-terminus YFP. **(B)** Co-infiltration of *RPP1-like* L*er R2*, *R3*, *R4*, *R8* with ATR1-δ51 Gw. Pictures in (A) and (B) were taken 48 h after infiltration. Samples for western blot analyses in (A) and (B) were collected 24 h after infiltration. No symptoms of cell death were observed at later time points of co-infiltration in (B).

Figure 9. QTL and GWAS mapping. **(A)** QTL mapping of disease resistance to *Hyaloperonospora arabidopsidis* (*Hpa*) isolate Gw in the L*er*/Sha recombinant inbred line (RIL) population (Clerkx et al., 2004), see **Supplemental Table 6**. The position of *RPP7* on chromosome 1 is indicated. **(B)** Manhattan plot of GWAS mapping for disease resistance to *Hpa* Gw in 288 accessions (see **Supplemental Table 8**). The list of most significant gene associations is shown in **Supplemental Table 9**.

SUPPLEMENTAL DATA

Supplemental Titles

Supplemental Figure 1. Leaf area **(A)** and trypan blue staining **(B)** in 5-week-old *sulki1*, *sulki2*, L*er*/Kas-2 NIL, cNIL (Alcázar et al., 2010) and parental accessions grown at 14 - 16ºC.

Supplemental Figure 2. Alignment of amino acid sequences for *RPP1-like* genes in L*er*, Col-0, Uk-1, Bla-1, and Ws.

Supplemental Figure 3. RT-qPCR expression analyses of *PR1* (right axis), *RPP1-like* L*er R2*, *R3*, *R4*, and *R8* genes (left axis) in L*er* plants treated with 100 µM BTH or 100 µM SA.

Supplemental Figure 4. CRISPR/Cas9-induced indel mutations in Cas9-*r2*, Cas9-*r3*, Cas9-*r4*, and Cas9-*r8* and their effects on protein translation.

Supplemental Figure 5. Leaf area **(A)** and trypan blue staining **(B)** of 5-week-old CRISPR/Cas9 *RPP1-like* L*er* mutants grown at 14 - 16ºC.

Supplemental Figure 6. Complementation of *sulki2-1* with *RPP1-like* L*er R3* gene reconstitutes L*er*/Kas-2 NIL phenotype.

Supplemental Figure 7. *PR1*, *EDS1* and *GST1* expression analyses in 5- and 7-week-old (w-o) Cas9 *r2-1*, *r2-2*, *r3-1*, *r3-2*, *r4-1*, *r4-2*, *r8-1* and *r8-2*, L*er*, Kas-2, L*er*/Kas-2 NIL and cNIL plants grown at 14 - 16ºC.

Supplemental Figure 8. Starch levels determined in leaves of 5-week old incompatible L*er*/Kas-2 NIL, Kas-2, L*er*, *sulki1-1*, *sulki1-7*, *sulki1-8* and *sulki1-9* grown at 14 - 16ºC.

Supplemental Figure 9. Apoplastic and vacuolar invertase activities of 5-week-old incompatible L*er*/Kas-2 NIL, Kas-2, L*er*, *sulki1-1*, *sulki1-7*, *sulki1-8*, and *sulki1-9* grown at 14 - 16ºC.

Supplemental Figure 10. Neighbor-joining phylogenetic analysis of ATR1 amino acid sequences from different *Hpa* isolates.

Supplemental Figure 11. Disease resistance phenotypes to *Hpa* Gw infection in different genotypes.

Supplemental Figure 12. Principal component analysis of the Gw population based on 134 genome-wide SNP.

Supplemental Figure 13. Coverage of Illumina reads mapping to the *At3g44400* - *At3g44480* interval in L*er*.

Supplemental Figure 14. *Quantile-Quantile* (Q–Q) plot for GWAS analysis of *Hpa* Gw disease resistance using the AMM method.

Supplemental Table 1. Segregation analyses of *sulki* and CRISPR/Cas9 mutants.

Supplemental Table 2. List of differentially expressed genes in the comparisons between Kas-2 *vs* L*er*/Kas-2 NIL and *sulki1-8 vs* L*er*/Kas-2 NIL and their gene ontology analyses.

Supplemental Table 3. List of metabolites and raw data from GC/MS analyses in L*er*/Kas-2 NIL, Kas-2, L*er*, *sulki1-1*, *sulki1-7*, *sulki1-8* and *sulki1-9*.

Supplemental Table 4. PC1 and PC2 loadings of L*er*/Kas-2 NIL, L*er*, Kas-2 and *sulki1* metabolite profiles.

Supplemental Table 5. Genotype data and disease resistance phenotypes to *Hpa* Gw infection in the Gorzów population.

Supplemental Table 6. Phenotype data for disease resistance to *Hpa* Gw in the L*er*/Sha RIL population. Genotype data of the L*er*/Sha RIL population used for QTL analyses.

Supplemental Table 7. List of *NLR* genes in the QTL interval of chromosome one for *Hpa* Gw disease resistance in the L*er*/Sha RIL population.

Supplemental Table 8. List of accessions used in GWAS mapping for disease resistance to *Hpa* Gw infection.
Supplemental Table 9. List of genes with highest associations in GWAS mapping for disease resistance to *Hpa* Gw.
Supplemental Table 10. Summary statistics of whole genome sequencing and RNA-seq reads.
Supplemental Table 11. List of oligonucleotides used in this work.

Supplemental Figure 1. Leaf area **(A)** and trypan blue staining **(B)** in 5-week-old *sulki1*, *sulki2*, L*er*/Kas-2 NIL, cNIL (Alcázar et al., 2010) and parental accessions grown at 14 - 16ºC. Error bars indicate standard deviation.

Supplemental Figure 2. Alignment of amino acid sequences for *RPP1-like* genes in L*er*, Col-0, Uk-1, Bla-1, and Ws. The position of amino acid variants in *sulki1* (*s1-1* to *s1-10*) mutants are shown on top and highlighted in yellow boxes within the aligned sequences.

Supplemental Figure 3. RT-qPCR expression analyses of *PR1* (right axis), *RPP1-like* L*er R2*, *R3*, *R4*, and *R8* genes (left axis) in L*er* plants treated with 100 µM BTH or 100 µM SA. Samples were harvested at 0 h, 0.5 h, 8 h and 24 h after SA, BTH or mock treatment. Values are relative to mock-treated samples and are the mean ± SD of three biological replicates, each with three technical replicates. Letters indicate values that are significantly different according to Student–Newman–Keuls test at *P* value <0.05.

Supplemental Figure 4. CRISPR/Cas9-induced indel mutations in Cas9-*r2*, Cas9-*r3*, Cas9-*r4*, and Cas9-*r8* and their effects on protein translation. TNL domains and motifs are shown in different colors or underlined.

Supplemental Figure 5. Leaf area **(A)** and trypan blue staining **(B)** of 5-week-old CRISPR/Cas9 *RPP1-like* L*er* mutants grown at 14 - 16ºC. **(C)** Trypan blue staining in 7-week-old plants. Error bars indicate standard deviation.

Supplemental Figure 6. Complementation of *sulki2-1* with *RPP1-like* L*er R3* gene reconstitutes L*er*/Kas-2 NIL phenotype. Pictures were taken 5 weeks after germination and growth at 14 - 16 ºC. Multiple independent *sulki2-1 RPP1-like* L*er R3* gene complemented lines (*sulki2-1 R3* L*er*) exhibited identical reconstitution of the phenotype. Quantitative expression analyses of *RPP1-like* L*er R3* in L*er*, *sulki2-1*, and one representative *sulki2-1 R3* L*er*. Error bars indicate standard deviation.

Supplemental Figure 7. *PR1*, *EDS1* and *GST1* expression analyses in 5- and 7-week-old (w-o) Cas9 *r2-1*, *r2-2*, *r3-1*, *r3-2*, *r4-1*, *r4-2*, *r8-1* and *r8-2*, L*er*, Kas-2, L*er*/Kas-2 NIL and cNIL plants grown at 14 - 16ºC. Error bars indicate standard deviation.

Supplemental Figure 8. Starch levels determined in leaves of 5-week old incompatible L*er*/Kas-2 NIL, Kas-2, L*er*, *sulki1-1*, *sulki1-7*, *sulki1-8* and *sulki1-9* grown at 14 - 16ºC. Letters indicate values that are significantly different according to Student–Newman–Keuls test at *P* value <0.05. FW, fresh weight. Error bars indicate standard deviation.

Supplemental Figure 9. Apoplastic and vacuolar invertase activities of 5-week-old incompatible L*er*/Kas-2 NIL, Kas-2, L*er*, *sulki1-1*, *sulki1-7*, *sulki1-8*, and *sulki1-9* grown at 14 - 16ºC. Letters indicate values that are significantly different according to Student–Newman–Keuls test at *P* value <0.05. FW, fresh weight. Error bars indicate standard deviation.

Supplemental Figure 10. Neighbor-joining phylogenetic analysis of ATR1 amino acid sequences from different *Hpa* isolates.

Supplemental Figure 11. Disease resistance phenotypes to *Hpa* Gw infection in different genotypes. L*er*, Col-0, Kas-2, L*er*/Kas-2 NIL, cNIL (Alcázar et al., 2010), Gw-159 (resistant genotype in the Gorzów population), Gw-16 (susceptible genotype in the Gorzów population), CRISPR/Cas9 NIL mutants, *eds1-2* (Feys et al. 2005), *nde1-1* (Stuttmann et al., 2016), L*er-NahG* (Bowling et al, 1997), *RPP1* and *RPP1-like* mutants in Col-0: *At3g44400* (N632237, N518154); *At3g44480* (N599581, N655327); *At3g44630* (N644159, N658450); *At3g44670* (N529707, N477722); *sid2-1* (Wildermuth et al., 2001).

Supplemental Figure 12. Principal component analysis of the Gw population based on 134 genome-wide SNP (see **Supplemental Table 5**). Resistant or susceptible genotypes to *Hpa* Gw are shown in black or red dots, respectively. Blue circles represent genotypes carrying conserved *RPP1-like* L*er* haplotypes.

Supplemental Figure 13. Coverage of Illumina reads mapping to the *At3g44400* - *At3g44480* interval in L*er*. Transposable elements are highlighted in yellow. The three digits next to the genes are identifiers for the last corresponding AGI numbers (*At3g44XXX*).

Supplemental Figure 14. *Quantile-Quantile* (Q–Q) plot for GWAS analysis of *Hpa* Gw disease resistance using the AMM method.

Supplemental Table 1. Segregation analyses of *sulki* and CRISPR/Cas9 mutants.

Supplemental Table 2. List of differentially expressed genes in the comparisons between Kas-2 *vs* L*er*/Kas-2 NIL and *sulki1-8 vs* L*er*/Kas-2 NIL and their gene ontology analyses. **(Supplemental Table 2-1)** Genes that exhibit significant expression differences in Kas-2 *vs* L*er*/Kas-2 NIL but no changes in *sulki1-8 vs* L*er*/Kas-2 NIL. **(Supplemental Table 2-2)** Genes which are up- or down-regulated in both Kas-2 *vs* L*er*/Kas-2 NIL and *sulki1-8 vs* L*er*/Kas-2 NIL. **(Supplemental Table 2-3)** Genes that exhibit significant expression differences in *sulki1-8 vs* L*er*/Kas-2 NIL but no changes in Kas-2 *vs* L*er*/Kas-2 NIL.

Supplemental Table 3. List of metabolites (**Supplemental Table 3-1**) and raw data (**Supplemental Table 3-2**) from GC/MS analyses in L*er*/Kas-2 NIL, Kas-2, L*er*, *sulki1-1*, *sulki1-7*, *sulki1-8* and *sulki1-9*.

Supplemental Table 4. PC1 and PC2 loadings of L*er*/Kas-2 NIL, L*er*, Kas-2 and *sulki1* metabolite profiles.

Supplemental Table 5. Genotype data and disease resistance phenotypes to *Hpa* Gw infection in the Gorzów population.

Supplemental Table 6. Phenotype data for disease resistance to *Hpa* Gw in the L*er*/Sha RIL population. Genotype data of the L*er*/Sha RIL population used for QTL analyses.

Supplemental Table 7. List of *NLR* genes in the QTL interval of chromosome one for *Hpa* Gw disease resistance in the L*er*/Sha RIL population.

Supplemental Table 8. List of accessions used in GWAS mapping for disease resistance to *Hpa* Gw infection (0, no sporulation; 1, sporulation only on cotyledons; 2, sporulation on cotyledons and fully expanded leaves).

Supplemental Table 9. List of genes with highest associations in GWAS mapping for disease resistance to *Hpa* Gw.

Supplemental Table 10. Summary statistics of whole genome sequencing and RNA-seq reads.

Supplemental Table 11. List of oligonucleotides used in this work.

REFERENCES

Aarts N, Metz M, Holub E, Staskawicz BJ, Daniels MJ, Parker JE (1998) Different requirements for EDS1 and NDR1 by disease resistance genes define at least two *R* gene-mediated signaling pathways in *Arabidopsis*. Proc Natl Acad Sci U S A **95**: 10306–10311

Alcázar R, García A V, Kronholm I, de Meaux J, Koornneef M, Parker JE, Reymond M (2010) Natural variation at *Strubbelig Receptor Kinase 3* drives immune-triggered incompatibilities between *Arabidopsis thaliana* accessions. Nat Genet **42**: 1135–1139

Alcázar R, García A V, Parker JE, Reymond M (2009) Incremental steps toward incompatibility revealed by *Arabidopsis* epistatic interactions modulating salicylic acid pathway activation. Proc Natl Acad Sci U S A **106**: 334–339

Alcázar R, Pecinka A, Aarts MGM, Fransz PF, Koornneef M (2012) Signals of speciation within *Arabidopsis thaliana* in comparison with its relatives. Curr Opin Plant Biol **15**: 205–211

Alcázar R, von Reth M, Bautor J, Chae E, Weigel D, Koornneef M, Parker JE (2014) Analysis of a plant complex *Resistance* gene locus underlying immune-related hybrid incompatibility and its occurrence in nature. PLoS Genet **10**: e1004848

Appeldoorn NJG, de Bruijn SM, Koot-Gronsveld EAM, Visser RGF, Vreugdenhil D, van der Plas LHW (1997) Developmental changes of enzymes involved in conversion of sucrose to hexose-phosphate during early tuberisation of potato. Planta **202**: 220–226

Ariga H, Katori T, Tsuchimatsu T, Hirase T, Tajima Y, Parker JE, Alcázar R, Koornneef M, Hoekenga O, Lipka AE, et al (2017) NLR locus-mediated trade-off between abiotic and biotic stress adaptation in *Arabidopsis*. Nat Plants **3**: 17072

Bakker EG, Toomajian C, Kreitman M, Bergelson J (2006) A genome-wide survey of *R* gene polymorphisms in *Arabidopsis*. Plant Cell **18**: 1803–1818

Bartsch M, Gobbato E, Bednarek P, Debey S, Schultze JL, Bautor J, Parker JE (2006) Salicylic acid-independent ENHANCED DISEASE SUSCEPTIBILITY1 signaling in *Arabidopsis* immunity and cell death is regulated by the monooxygenase FMO1 and the Nudix hydrolase NUDT7. Plant Cell **18**: 1038–1051

Bernoux M, Ve T, Williams S, Warren C, Hatters D, Valkov E, Zhang X, Ellis JG, Kobe B, Dodds PN (2011) Structural and functional analysis of a plant resistance protein TIR domain reveals interfaces for self-association, signaling, and autoregulation. Cell Host Microbe **9**: 200–211

Bolton MD (2009) Primary metabolism and plant defense - fuel for the fire. Mol Plant-Microbe Interact **22**: 487–497

Bomblies K (2010) Doomed lovers: mechanisms of isolation and incompatibility in plants. Annu Rev Plant Biol **61**: 109–124

Bomblies K, Lempe J, Epple P, Warthmann N, Lanz C, Dangl JL, Weigel D (2007) Autoimmune response as a mechanism for a Dobzhansky-Muller-type incompatibility syndrome in plants. PLoS Biol **5**: e236

Bomblies K, Weigel D (2007) Hybrid necrosis: autoimmunity as a potential gene-flow barrier in plant species. Nat Rev Genet **8**: 382–393

Botella MA, Parker JE, Frost LN, Bittner-Eddy PD, Beynon JL, Daniels MJ, Holub EB, Jones JD (1998) Three genes of the *Arabidopsis RPP1* complex resistance locus recognize distinct *Peronospora parasitica* avirulence determinants. Plant Cell **10**: 1847–1860

Bowling SA, Guo A, Cao H, Gordon AS, Klessig DF, Dong X (1994) A mutation in *Arabidopsis* that leads to constitutive expression of systemic acquired resistance. Plant Cell **6**: 1845–1857

Cao J, Schneeberger K, Ossowski S, Günther T, Bender S, Fitz J, Koenig D, Lanz C, Stegle O, Lippert C, et al (2011) Whole-genome sequencing of multiple *Arabidopsis thaliana* populations. Nat Genet **43**: 956–963

Chae E, Bomblies K, Kim S-TT, Karelina D, Zaidem M, Ossowski S, Martín-Pizarro C, Laitinen RAEAE, Rowan BAA, Tenenboim H, et al (2014) Species-wide genetic incompatibility analysis identifies immune genes as hot spots of deleterious epistasis. Cell **159**: 1341–1351

Chen C, Chen H, Lin Y-S, Shen J-B, Shan J-X, Qi P, Shi M, Zhu M-Z, Huang X-H, Feng Q, et al (2014) A two-locus interaction causes interspecific hybrid weakness in rice. Nat Commun **5**: 3357

Clerkx EJM, El-Lithy ME, Vierling E, Ruys GJ, Blankestijn-De Vries H, Groot SPC, Vreugdenhil D, Koornneef M (2004) Analysis of natural allelic variation of Arabidopsis seed germination and seed longevity traits between the accessions Landsberg *erecta* and Shakdara, using a new recombinant inbred line population. PLANT Physiol **135**: 432–443

Coates ME, Beynon JL (2010) *Hyaloperonospora arabidopsidis* as a pathogen model. Annu Rev Phytopathol **48**: 329–345

Coyne JA, Orr HA (2004) Speciation. Sinauer Associates

Coyne JJA (1992) Genetics and speciation. Nature **355**: 511–515

Dettman JR, Sirjusingh C, Kohn LM, Anderson JB (2007) Incipient speciation by divergent adaptation and antagonistic epistasis in yeast. Nature **447**: 585–588

Dodds PN, Rathjen JP (2010) Plant immunity: towards an integrated view of plant-pathogen interactions. Nat Rev Genet **11**: 539–548

Doyle J (1991) DNA protocols for plants. Mol. Tech. Taxon. Springer Berlin Heidelberg, Berlin, Heidelberg, pp 283–293

Earley KW, Haag JR, Pontes O, Opper K, Juehne T, Song K, Pikaard CS (2006) Gateway-compatible vectors for plant functional genomics and proteomics. Plant J **45**: 616–629

Falk A, Feys BJ, Frost LN, Jones JD, Daniels MJ, Parker JE (1999) EDS1, an essential component of R gene-mediated disease resistance in *Arabidopsis* has homology to eukaryotic lipases. Proc Natl Acad Sci U S A **96**: 3292–3297

Fauser F, Schiml S, Puchta H (2014) Both CRISPR/Cas-based nucleases and nickases can be used efficiently for genome engineering in *Arabidopsis thaliana*. Plant J **79**: 348–359

Feys BJ, Moisan LJ, Newman MA, Parker JE (2001) Direct interaction between the *Arabidopsis* disease resistance signaling proteins, EDS1 and PAD4. EMBO J **20**: 5400–5411

Feys BJ, Wiermer M, Bhat RA, Moisan LJ, Medina-Escobar N, Neu C, Cabral A, Parker JE (2005) Arabidopsis SENESCENCE-ASSOCIATED GENE101 stabilizes and signals within an ENHANCED DISEASE SUSCEPTIBILITY1 complex in plant innate immunity. Plant Cell **17**: 2601–2613

Flynn KM, Cooper TF, Moore FB-G, Cooper VS (2013) The environment affects epistatic interactions to alter the topology of an empirical fitness landscape. PLoS Genet **9**: e1003426

Goritschnig S, Steinbrenner AD, Grunwald DJ, Staskawicz BJ (2016) Structurally distinct *Arabidopsis thaliana* NLR immune receptors recognize tandem WY domains of an oomycete effector. New Phytol **210**: 984–996

Hurwitz BL, Kudrna D, Yu Y, Sebastian A, Zuccolo A, Jackson SA, Ware D, Wing RA, Stein L (2010) Rice structural variation: a comparative analysis of structural variation between rice and three of its closest relatives in the genus Oryza. Plant J **63**: 990–1003

Jeuken MJW, Zhang NW, McHale LK, Pelgrom K, den Boer E, Lindhout P, Michelmore RW, Visser RGF, Niks RE (2009) RIN4 causes hybrid necrosis and race-specific resistance in an interspecific lettuce hybrid. Plant Cell **21**: 3368–3378

Kang HM, Sul JH, Service SK, Zaitlen NA, Kong S, Freimer NB, Sabatti C, Eskin E (2010) Variance component model to account for sample structure in genome-wide association studies. Nat Genet **42**: 348–354

Khan M, Subramaniam R, Desveaux D (2016) Of guards, decoys, baits and traps: pathogen perception in plants by type III effector sensors. Curr Opin Microbiol **29**: 49–55

Kopka J, Schauer N, Krueger S, Birkemeyer C, Usadel B, Bergmuller E, Dormann P, Weckwerth W, Gibon Y, Stitt M, et al (2005) GMD@CSB.DB: the Golm Metabolome Database. Bioinformatics **21**: 1635–1638

Krasileva K V, Dahlbeck D, Staskawicz BJ (2010) Activation of an *Arabidopsis* resistance protein is specified by the in planta association of its leucine-rich repeat domain with the cognate oomycete effector. Plant Cell **22**: 2444–2458

Krüger J, Thomas CM, Golstein C, Dixon MS, Smoker M, Tang S, Mulder L, Jones JDG (2002) A tomato cysteine protease required for Cf-2-dependent disease resistance and suppression of autonecrosis. Science **296**:744-747

McDowell JM, Cuzick A, Can C, Beynon J, Dangl JL, Holub EB (2000) Downy mildew (*Peronospora parasitica*) resistance genes in *Arabidopsis* vary in functional requirements for NDR1, EDS1, NPR1 and salicylic acid accumulation. Plant J **22**: 523–529

McHale LK, Haun WJ, Xu WW, Bhaskar PB, Anderson JE, Hyten DL, Gerhardt DJ, Jeddeloh JA, Stupar RM (2012) Structural variants in the soybean genome localize to clusters of biotic stress-response genes. Plant Physiol **159**: 1295–1308

Meyers BC, Kozik A, Griego A, Kuang H, Michelmore RW (2003) Genome-wide analysis of NBS-LRR-encoding genes in *Arabidopsis*. Plant Cell **15**: 809–34

Muñoz-Amatriaín M, Eichten SR, Wicker T, Richmond TA, Mascher M, Steuernagel B, Scholz U, Ariyadasa R, Spannagl M, Nussbaumer T, et al (2013) Distribution, functional impact, and origin mechanisms of copy number variation in the barley genome. Genome Biol **14**: R58

Ono J, Gerstein AC, Otto SP, Walker S, Stewart-Ornstein J, Newman H (2017) Widespread genetic incompatibilities between first-step mutations during parallel adaptation of *Saccharomyces cerevisiae* to a common environment. PLoS Biol **15**: e1002591

van Ooijen G, Mayr G, Kasiem MM a, Albrecht M, Cornelissen BJC, Takken FLW (2008) Structure-function analysis of the NB-ARC domain of plant disease resistance proteins. J Exp Bot **59**: 1383–1397

Rehmany AP, Gordon A, Rose LE, Allen RL, Armstrong MR, Whisson SC, Kamoun S, Tyler BM, Birch PRJ, Beynon JL (2005) Differential recognition of highly divergent downy mildew avirulence gene alleles by *RPP1* resistance genes from two *Arabidopsis* lines. Plant Cell **17**: 1839–1850

Schreiber KJ, Bentham A, Williams SJ, Kobe B, Staskawicz BJ, Meng E (2016) Multiple domain associations within the *Arabidopsis* immune receptor RPP1 regulate the activation of programmed cell death. PLoS Pathog **12**: e1005769

Seren Ü, Vilhjálmsson BJ, Horton MW, Meng D, Forai P, Huang YS, Long Q, Segura V, Nordborg M (2012) GWAPP: a web application for genome-wide association mapping in *Arabidopsis*. Plant Cell **24**: 4793–4805

Sherlock G, Petrov DA, Levy S, Agarwala A, Chang J, Ebel E (2017) Seeking goldilocks during evolution of drug resistance. PLoS Biol **15**: e2001872

Sicard A, Kappel C, Josephs EB, Lee YW, Marona C, Stinchcombe JR, Wright SI, Lenhard M (2015) Divergent sorting of a balanced ancestral polymorphism underlies the establishment of gene-flow barriers in Capsella. Nat Commun **6**: 7960

Smith AM, Zeeman SC (2006) Quantification of starch in plant tissues. Nat Protoc **1**: 1342–1345

Sohn KH, Lei R, Nemri A, Jones JDG (2007) The downy mildew effector proteins ATR1 and ATR13 promote disease susceptibility in *Arabidopsis thaliana*. Plant Cell **19**: 4077–4090

Steinbrenner AD, Goritschnig S, Staskawicz BJ (2015) Recognition and activation domains contribute to allele-specific responses of an Arabidopsis NLR receptor to an oomycete effector protein. PLoS Pathog **11**: e1004665

Stuttmann J, Peine N, Garcia A V., Wagner C, Choudhury SR, Wang Y, Velikkakam James G, Griebel T, Alcázar R, Tsuda K, et al (2016) *Arabidopsis thaliana* DM2h (R8) within the Landsberg *RPP1-like* resistance locus underlies three different cases of EDS1- conditioned autoimmunity. PLoS Genet **12**: e1005990

Sukarta OCA, Slootweg EJ, Goverse A (2016) Structure-informed insights for NLR functioning in plant immunity. Semin Cell Dev Biol **56**: 134–149

Swiderski MR, Birker D, Jones JDG (2009) The TIR domain of TIR-NB-LRR resistance proteins is a signaling domain involved in cell death induction. Mol Plant-Microbe Interact **22**: 157–165

Takken FLW, Goverse A (2012) How to build a pathogen detector: structural basis of NB-LRR function. Curr Opin Plant Biol **15**: 375–384

Tauzin AS, Giardina T (2014) Sucrose and invertases, a part of the plant defense response to the biotic stresses. Front Plant Sci **5**: 293

Wildermuth MC, Dewdney J, Wu G, Ausubel FM (2001) Isochorismate synthase is required to synthesize salicylic acid for plant defence. Nature **414**: 562–565

Williams SJ, Sohn KH, Wan L, Bernoux M, Sarris PF, Segonzac C, Ve T, Ma Y, Saucet SB, Ericsson DJ, et al (2014) Structural basis for assembly and function of a heterodimeric plant immune receptor. Science **344**: 299–303

Xu X, Liu X, Ge S, Jensen JD, Hu F, Li X, Dong Y, Gutenkunst RN, Fang L, Huang L, et al (2011) Resequencing 50 accessions of cultivated and wild rice yields markers for identifying agronomically important genes. Nat Biotechnol **30**: 105–111

Yamamoto E, Takashi T, Morinaka Y, Lin S, Wu J, Matsumoto T, Kitano H, Matsuoka M, Ashikari M (2010) Gain of deleterious function causes an autoimmune response and Bateson-Dobzhansky-Muller incompatibility in rice. Mol Genet Genomics **283**: 305–315

Yuan J, He SY (1996) The *Pseudomonas syringae* Hrp regulation and secretion system controls the production and secretion of multiple extracellular proteins. J Bacteriol **178**: 6399–6402

Zarza X, Atanasov KE, Marco F, Arbona V, Carrasco P, Kopka J, Fotopoulos V, Munnik T, Gómez-Cadenas A, Tiburcio AF, et al (2017) *Polyamine oxidase 5* loss-of-function mutations in *Arabidopsis thaliana* trigger metabolic and transcriptional reprogramming and promote salt stress tolerance. Plant Cell Environ **40**: 527–542

Zhang X, Bernoux M, Bentham AR, Newman TE, Ve T, Casey LW, Raaymakers TM, Hu J, Croll TI, Schreiber KJ, et al (2017) Multiple functional self-association interfaces in plant TIR domains. Proc Natl Acad Sci **114**: E2046–E2052

Zhang Z, Ersoz E, Lai C-Q, Todhunter RJ, Tiwari HK, Gore MA, Bradbury PJ, Yu J, Arnett DK, Ordovas JM, et al (2010) Mixed linear model approach adapted for genome-wide association studies. Nat Genet **42**: 355–360

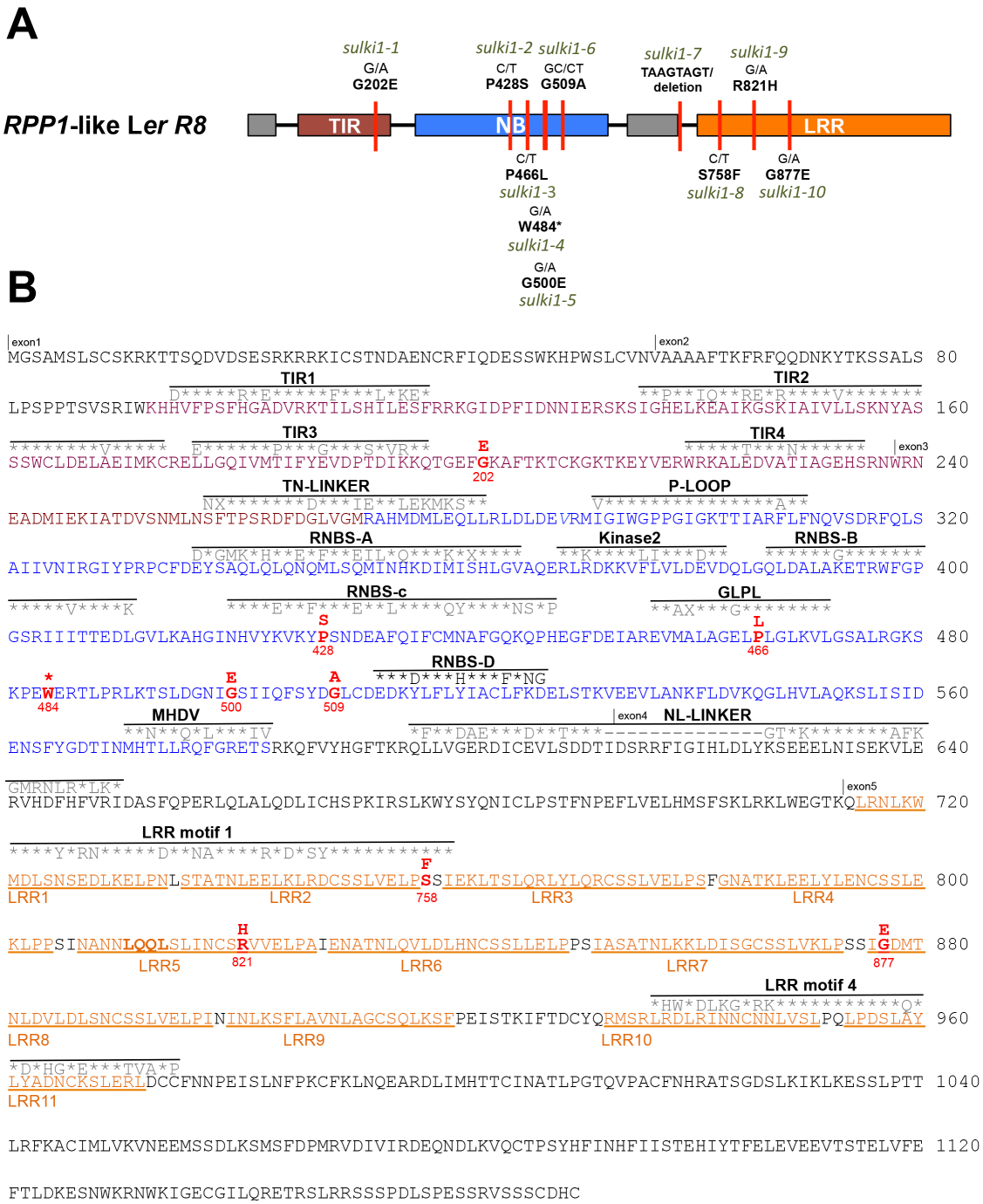

Figure 1. *sulki1* mutations mapping to *RPP1*-like *R8 Ler*. **(A)** Schematic representation of non-synonymous substitutions identified in *sulki1* mutants. Exon/intron organization and Toll-interleukin receptor (TIR), nucleotide binding (NB) and leucine rich repeat (LRR) domains are shown. **(B)** Detailed representation of *RPP1*-like *R8 Ler* amino acid sequence, conserved motifs (Meyers et al., 2003) and position of *sulki1* mutations.

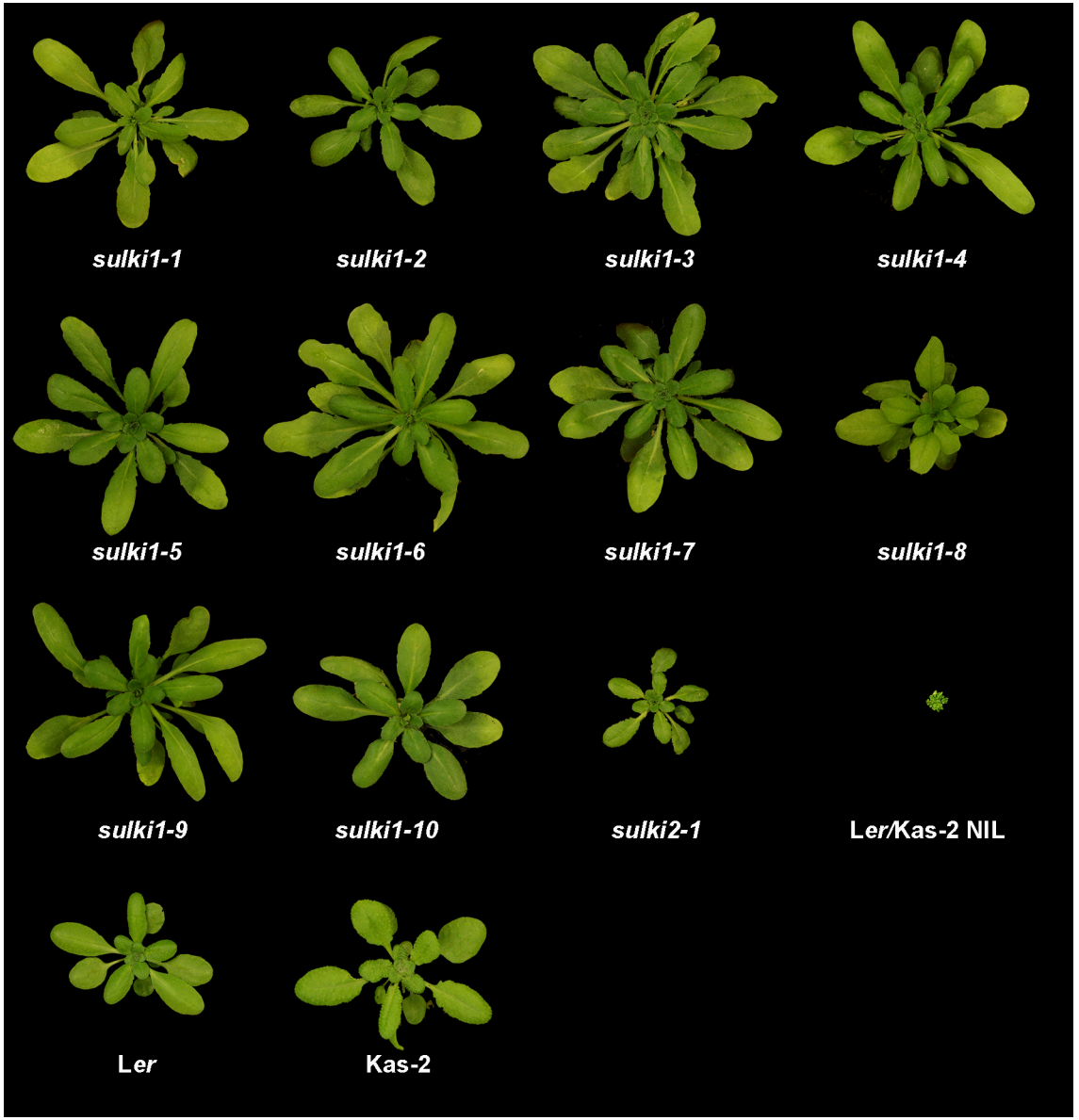

Figure 2. Growth phenotypes of 5-week old *sulki1*, *sulki2*, L*er*/Kas-2 NIL grown at 14 - 16 °C under 12 h light / 12 h dark cycles and light intensity of 120 µmol/m^2sec.

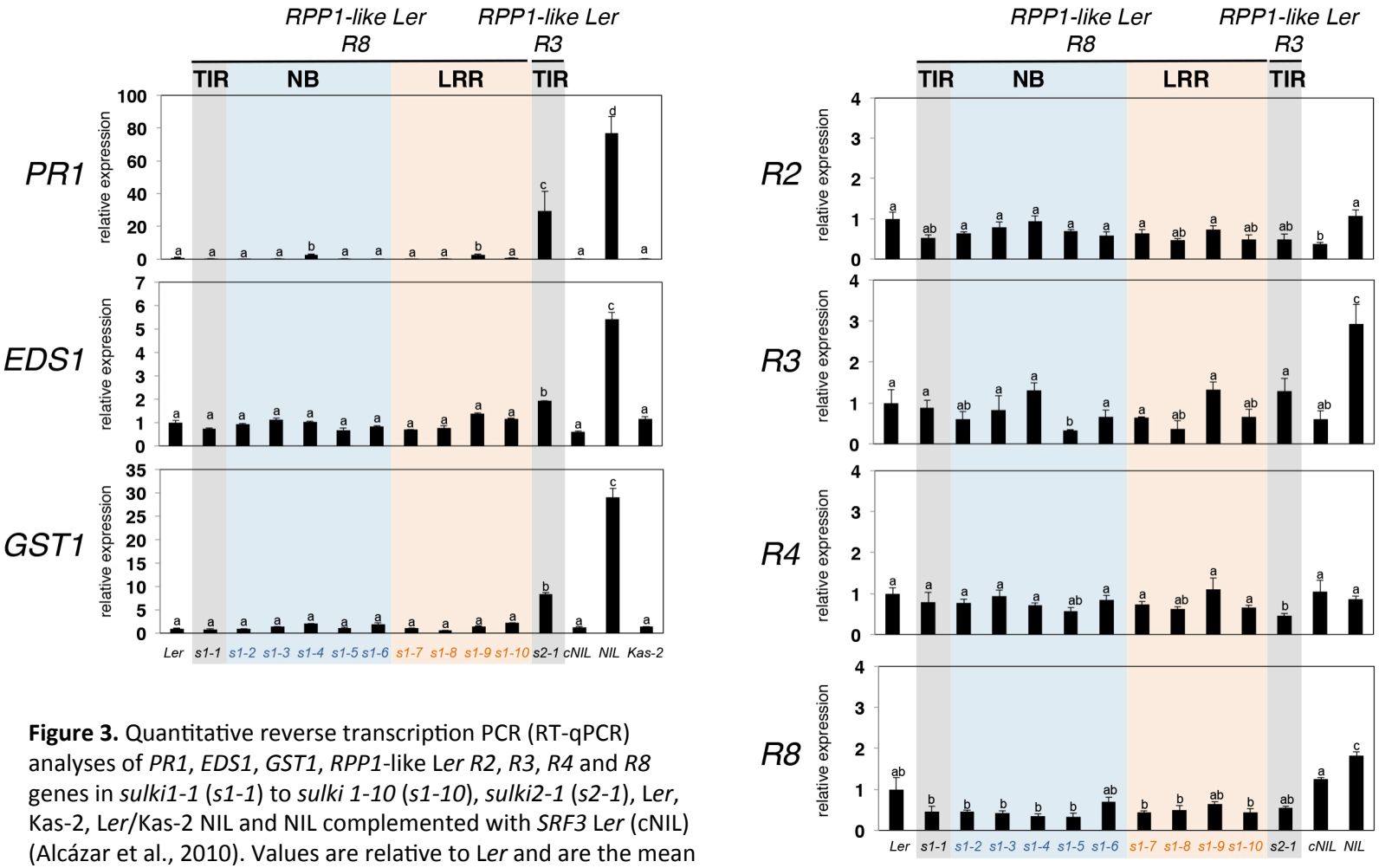

Figure 3. Quantitative reverse transcription PCR (RT-qPCR) analyses of *PR1*, *EDS1*, *GST1*, *RPP1*-like L*er R2*, *R3*, *R4* and *R8* genes in *sulki1-1* (*s1-1*) to *sulki 1-10* (*s1-10*), *sulki2-1* (*s2-1*), L*er*, Kas-2, L*er*/Kas-2 NIL and NIL complemented with *SRF3* L*er* (cNIL) (Alcázar et al., 2010). Values are relative to L*er* and are the mean ± SD of three biological replicates, each with three technical replicates. Letters indicate values that are significantly different according to Student–Newman–Keuls test at *P* value <0.05.

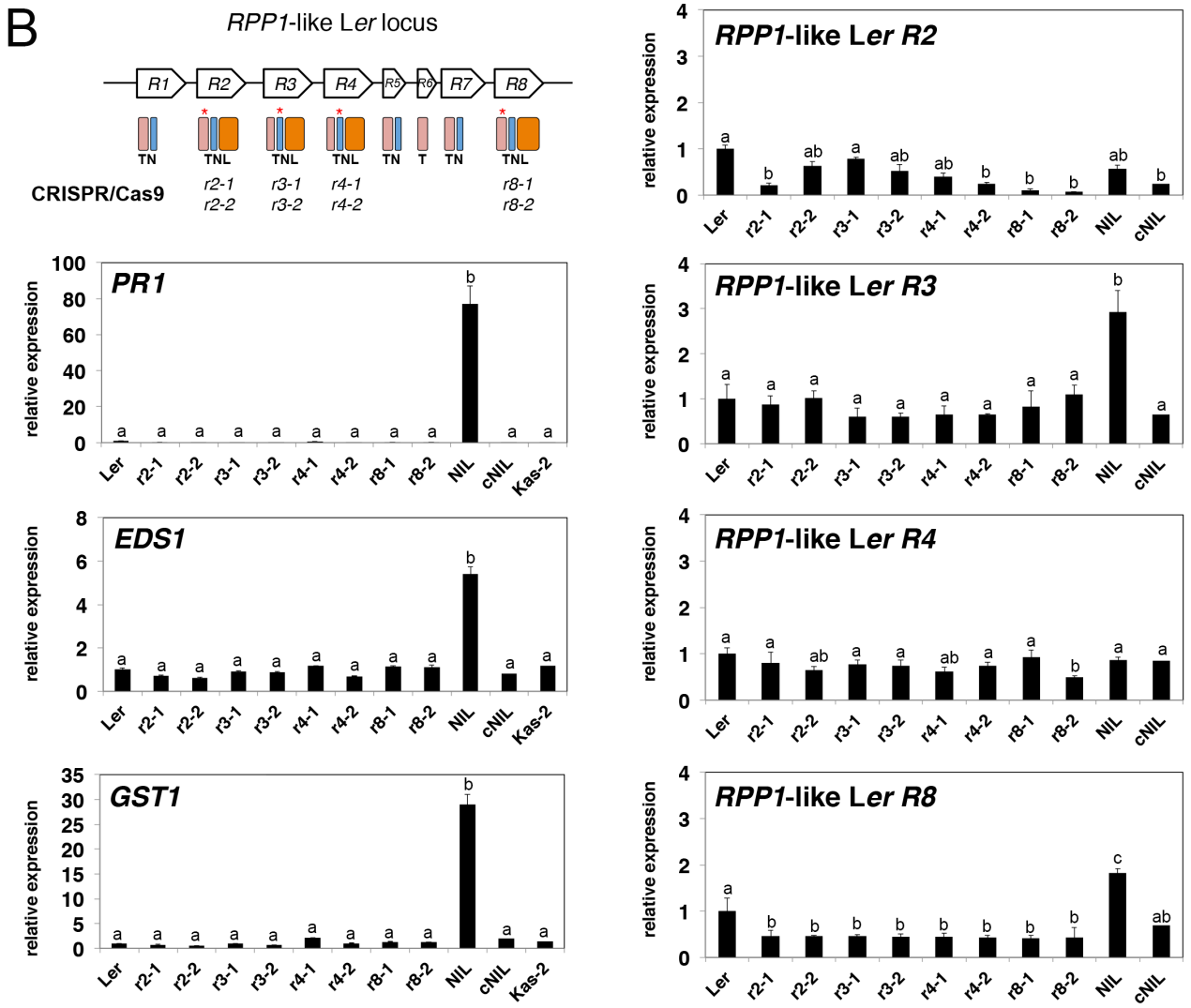

Figure 4. (A) Phenotypes of 5-week old Cas9-*r2-1*, Cas9-*r3-1*, Cas9-*r4-1*, Cas9-*r8-1* mutants in the L*er*/Kas-2 NIL background, L*er*/Kas-2 NIL and parental lines (L*er* and Kas-2) grown at 14 -16 °C. The position of stop codons in TIR (T) or NB (N) domains of *RPP1*-like genes is marked with an asterisk. **(B)** Gene expression analyses of *PR1*, *EDS1*, *GST1*, *RPP1*-like L*er R2*, *R3*, *R4* and *R8* in Cas9 *r2-1*, *r2-2*, *r3-1*, *r3-2*, *r4-1*, *r4-2*, *r8-1* and *r8-2* mutant alleles, L*er*, Kas-2, L*er*/Kas-2 NIL and cNIL plants grown at 14 - 16 °C during five weeks. Analyses were performed as described in **Fig. 3**.

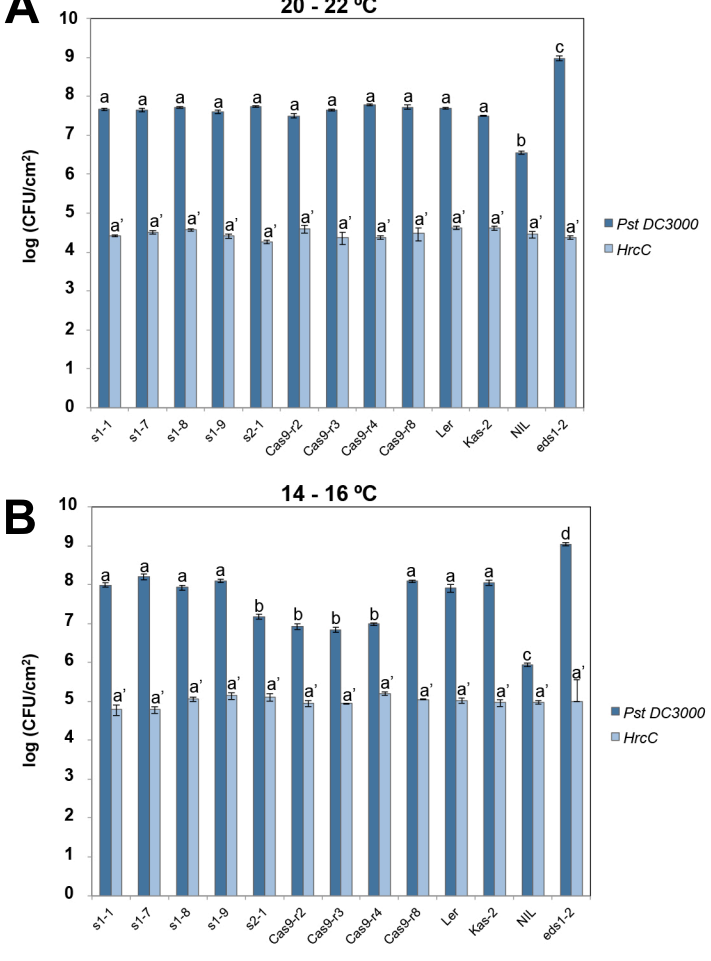
A
20 - 22 ºC
log (CFU/cm²)
Pst DC3000
HrcC
s1-1
s1-7
s1-8
s1-9
s2-1
Cas9-r2
Cas9-r3
Cas9-r4
Cas9-r8
Ler
Kas-2
NIL
eds1-2
B
14 - 16 ºC
log (CFU/cm²)
Pst DC3000
HrcC

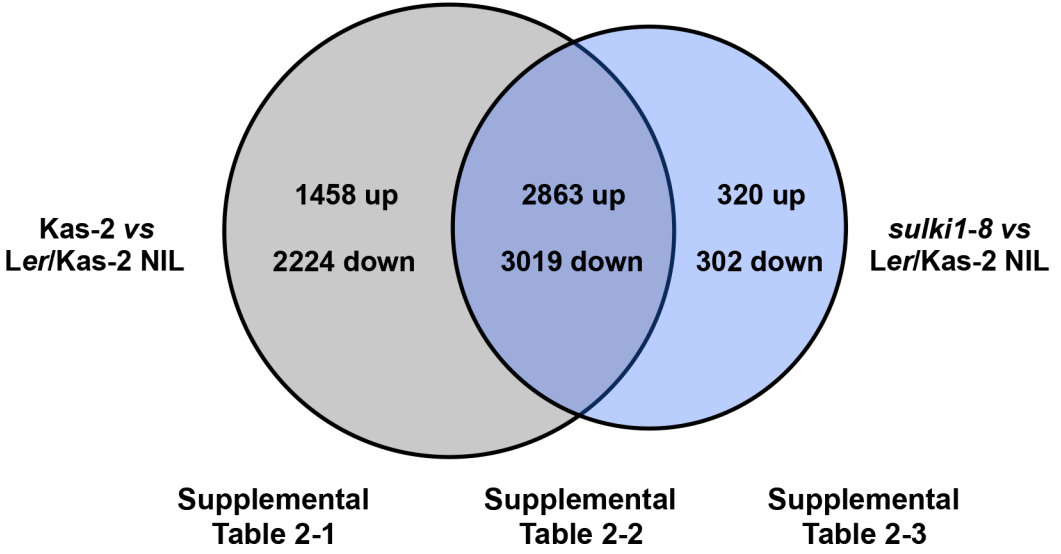
Kas-2 *vs*
L*er*/Kas-2 NIL
1458 up
2224 down
2863 up
3019 down
320 up
302 down
sulki1-8 vs
L*er*/Kas-2 NIL
Supplemental
Table 2-1
Supplemental
Table 2-2
Supplemental
Table 2-3

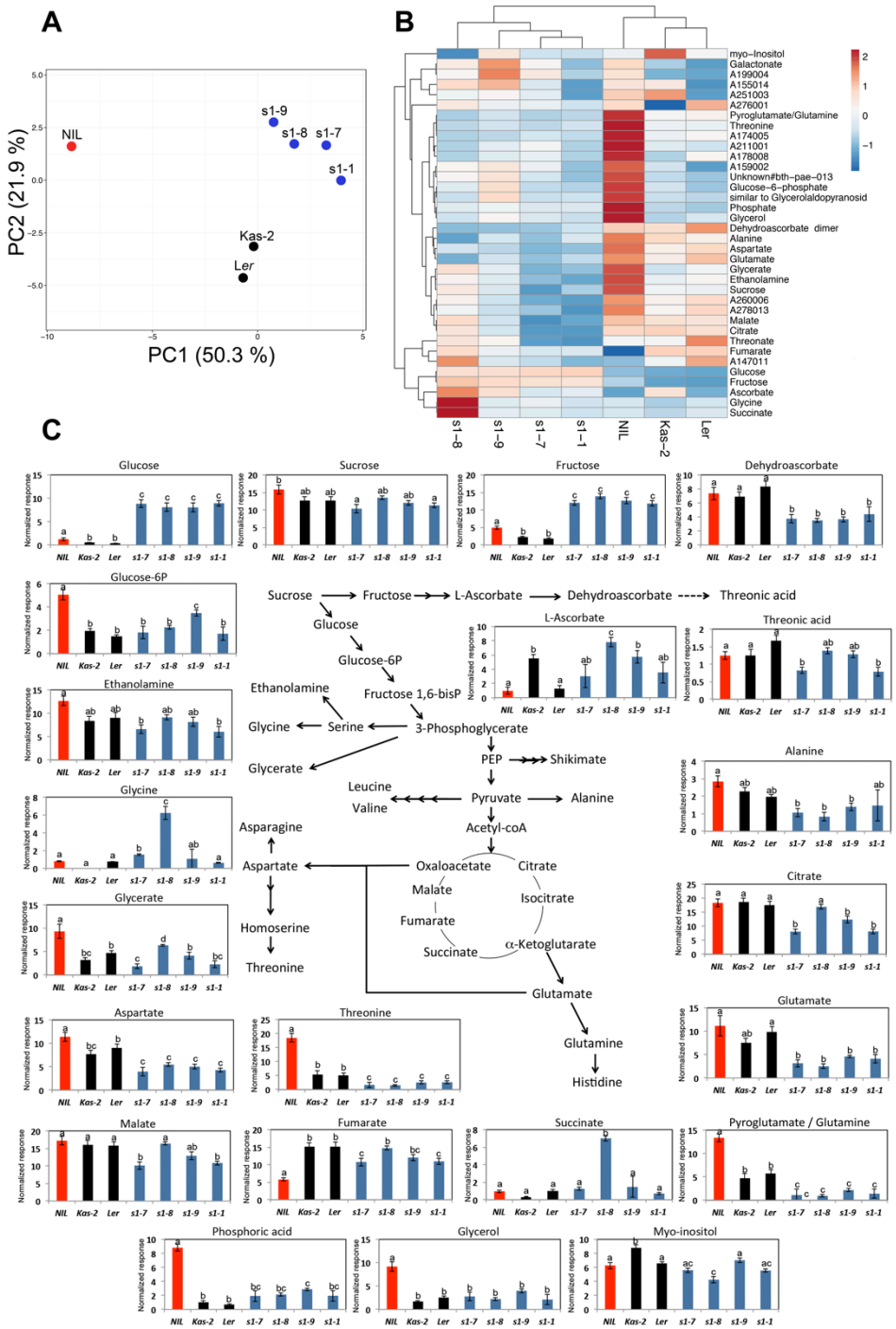

Figure 7. (A) Principal component analysis and **(B)** Hierarchical cluster analysis (*HCA*) with Pearson's correlation and average linkage of samples and metabolites from 5-week old *sulki1-1* (*s1-1*), *sulki1-7* (*s1-7*), *sulki1-8* (*s1-8*), *sulki1-9* (*s1-9*), L*er*, Kas-2 and Ler/Kas-2 NIL plants grown at 14-16 °C. **(C)** Log_2 normalized responses for some metabolites determined by GC/MS in the above genotypes, and schematic representation of their metabolic pathways. Different letters indicate significant differences ($P < 0.01$) in a Student-Newman Keuls test. Error bars, s.d. A complete list of analyzed metabolites is provided in **Supplementary Table S3**.

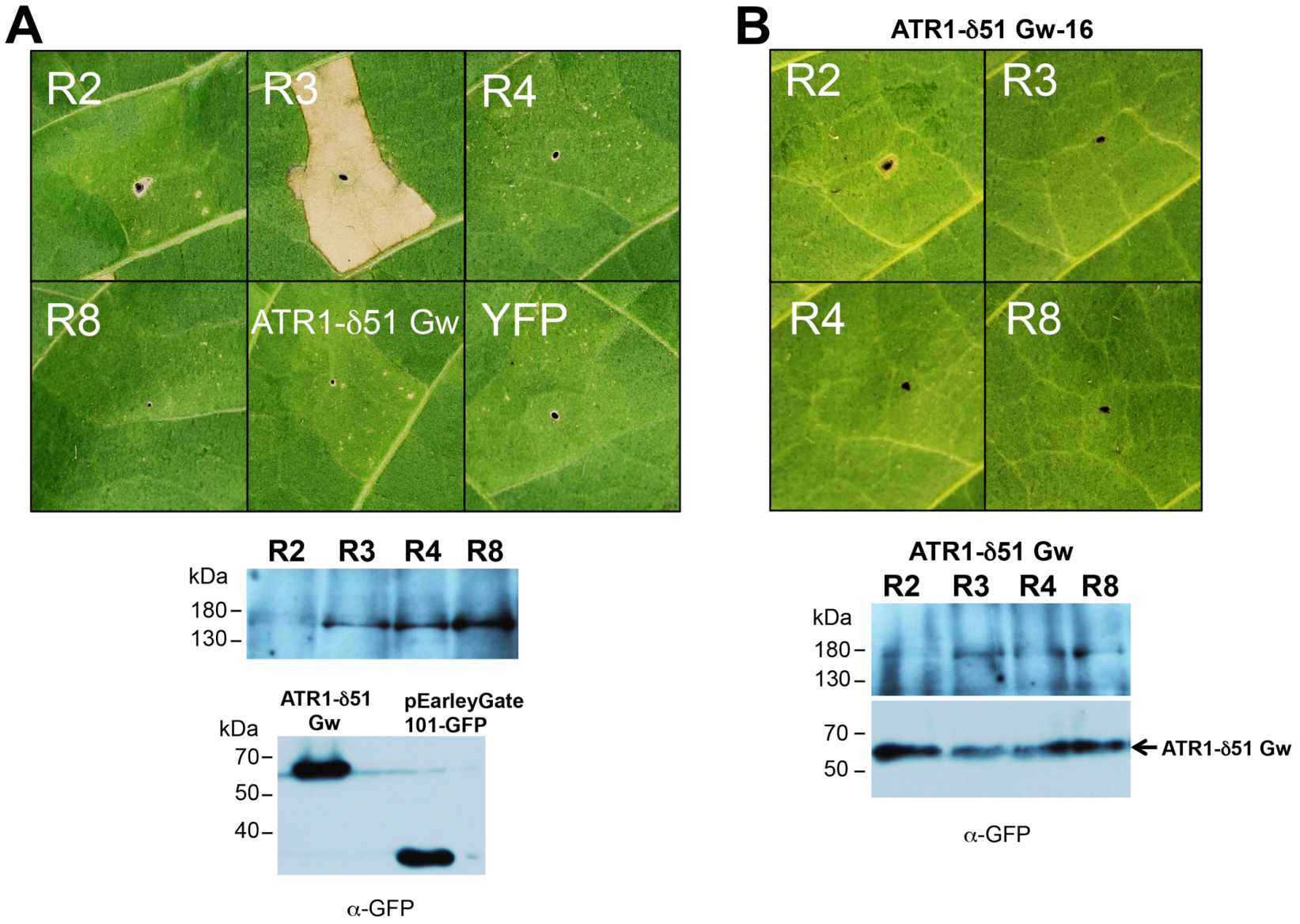

Figure 8. Transient expression assays in *Nicotiana tabacum*. **(A)** Transient expression of genomic versions of 35s: *RPP1*-like L*er R2*, *R3*, *R4*, *R8* and ATR1-d51 Gw, tagged with C-terminus YFP. **(B)** Co-infiltration of *RPP1*-like L*er R2*, *R3*, *R4*, *R8* with ATR1-d51 Gw. Pictures in (A) and (B) were taken 48 h after infiltration. Samples for western blot analyses in (A) and (B) were collected 24 h after infiltration. No symptoms of cell death were observed at later time points of co-infiltration in (B).

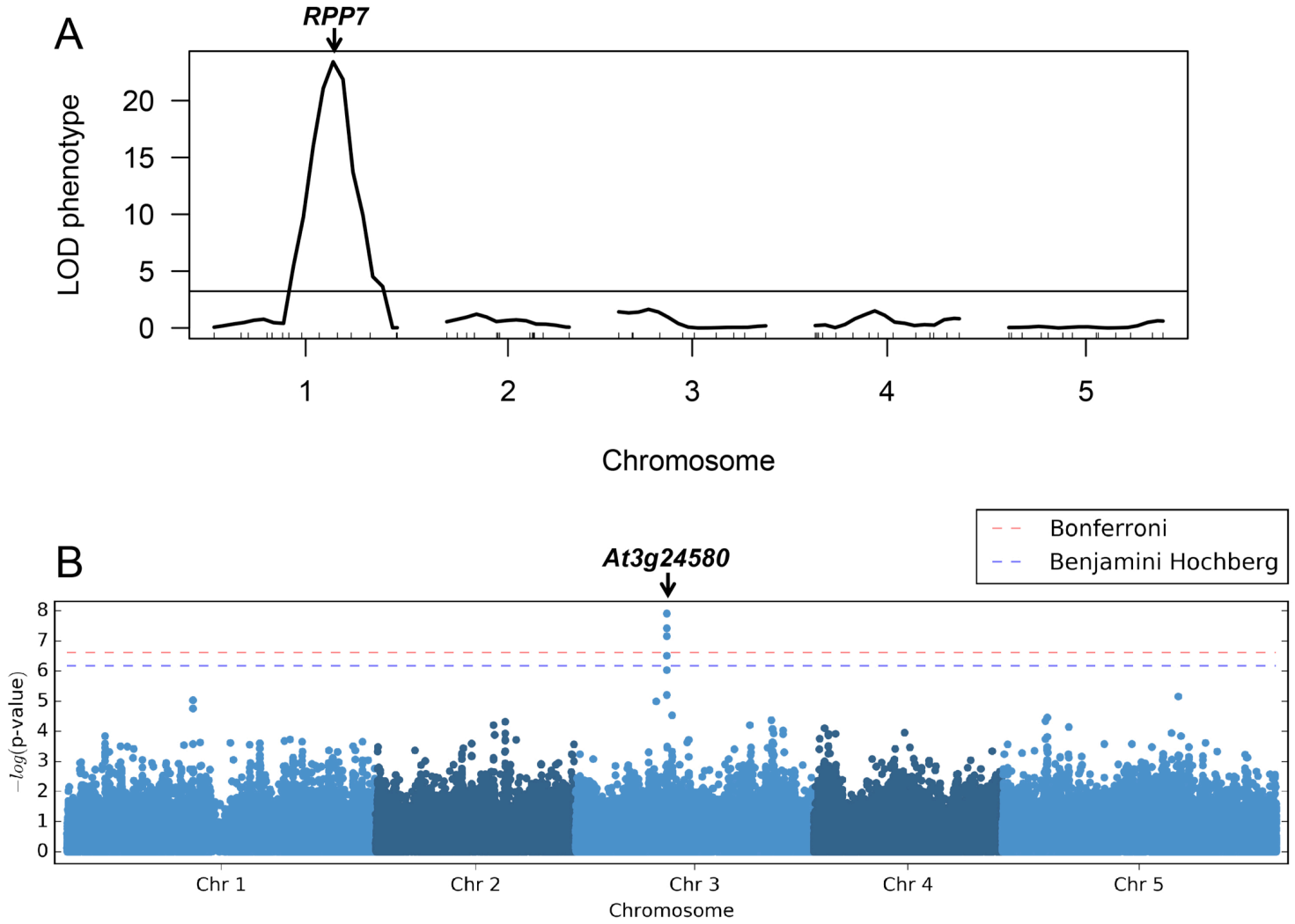

Figure 9. (A) QTL mapping of disease resistance to *Hyaloperonospora arabidopsidis* (*Hpa*) isolate Gw in the L*er*/Sha recombinant inbred line (RIL) population (Clerkx et al., 2004), see **Supplementary Table S6**. Position of *RPP7* on chromosome 1 is indicated. **(B)** Manhattan plot of GWAS mapping for disease resistance to *Hpa* Gw in 288 accessions (see **Supplementary Table S8**). List with most significant gene associations is shown in **Supplementary Table S9**.

Parsed Citations

Aarts N, Metz M, Holub E, Staskawicz BJ, Daniels MJ, Parker JE (1998) Different requirements for EDS1 and NDR1 by disease resistance genes define at least two R gene-mediated signaling pathways in Arabidopsis. Proc Natl Acad Sci U S A 95: 10306–10311
Pubmed: Author and Title
Google Scholar: Author Only Title Only Author and Title

Alcázar R, García AV, Kronholm I, de Meaux J, Koornneef M, Parker JE, Reymond M (2010) Natural variation at Strubbelig Receptor Kinase 3 drives immune-triggered incompatibilities between Arabidopsis thaliana accessions. Nat Genet 42: 1135–1139
Pubmed: Author and Title
Google Scholar: Author Only Title Only Author and Title

Alcázar R, García AV, Parker JE, Reymond M (2009) Incremental steps toward incompatibility revealed by Arabidopsis epistatic interactions modulating salicylic acid pathway activation. Proc Natl Acad Sci U S A 106: 334–339
Pubmed: Author and Title
Google Scholar: Author Only Title Only Author and Title

Alcázar R, Pecinka A, Aarts MGM, Fransz PF, Koornneef M (2012) Signals of speciation within Arabidopsis thaliana in comparison with its relatives. Curr Opin Plant Biol 15: 205–211
Pubmed: Author and Title
Google Scholar: Author Only Title Only Author and Title

Alcázar R, von Reth M, Bautor J, Chae E, Weigel D, Koornneef M, Parker JE (2014) Analysis of a plant complex Resistance gene locus underlying immune-related hybrid incompatibility and its occurrence in nature. PLoS Genet 10: e1004848
Pubmed: Author and Title
Google Scholar: Author Only Title Only Author and Title

Appeldoorn NJG, de Bruijn SM, Koot-Gronsveld EAM, Visser RGF, Vreugdenhil D, van der Plas LHW (1997) Developmental changes of enzymes involved in conversion of sucrose to hexose-phosphate during early tuberisation of potato. Planta 202: 220–226
Pubmed: Author and Title
Google Scholar: Author Only Title Only Author and Title

Ariga H, Katori T, Tsuchimatsu T, Hirase T, Tajima Y, Parker JE, Alcázar R, Koornneef M, Hoekenga O, Lipka AE, et al (2017) NLR locus-mediated trade-off between abiotic and biotic stress adaptation in Arabidopsis. Nat Plants 3: 17072
Pubmed: Author and Title
Google Scholar: Author Only Title Only Author and Title

Bakker EG, Toomajian C, Kreitman M, Bergelson J (2006) A genome-wide survey of R gene polymorphisms in Arabidopsis. Plant Cell 18: 1803–1818
Pubmed: Author and Title
Google Scholar: Author Only Title Only Author and Title

Bartsch M, Gobbato E, Bednarek P, Debey S, Schultze JL, Bautor J, Parker JE (2006) Salicylic acid-independent ENHANCED DISEASE SUSCEPTIBILITY1 signaling in Arabidopsis immunity and cell death is regulated by the monooxygenase FMO1 and the Nudix hydrolase NUDT7. Plant Cell 18: 1038–1051
Pubmed: Author and Title
Google Scholar: Author Only Title Only Author and Title

Bernoux M, Ve T, Williams S, Warren C, Hatters D, Valkov E, Zhang X, Ellis JG, Kobe B, Dodds PN (2011) Structural and functional analysis of a plant resistance protein TIR domain reveals interfaces for self-association, signaling, and autoregulation. Cell Host Microbe 9: 200–211
Pubmed: Author and Title
Google Scholar: Author Only Title Only Author and Title

Bolton MD (2009) Primary metabolism and plant defense - fuel for the fire. Mol Plant-Microbe Interact 22: 487–497
Pubmed: Author and Title
Google Scholar: Author Only Title Only Author and Title

Bomblies K (2010) Doomed lovers: mechanisms of isolation and incompatibility in plants. Annu Rev Plant Biol 61: 109–124
Pubmed: Author and Title
Google Scholar: Author Only Title Only Author and Title

Bomblies K, Lempe J, Epple P, Warthmann N, Lanz C, Dangl JL, Weigel D (2007) Autoimmune response as a mechanism for a Dobzhansky-Muller-type incompatibility syndrome in plants. PLoS Biol 5: e236
Pubmed: Author and Title
Google Scholar: Author Only Title Only Author and Title

Bomblies K, Weigel D (2007) Hybrid necrosis: autoimmunity as a potential gene-flow barrier in plant species. Nat Rev Genet 8: 382–393
Pubmed: Author and Title
Google Scholar: Author Only Title Only Author and Title

Botella MA, Parker JE, Frost LN, Bittner-Eddy PD, Beynon JL, Daniels MJ, Holub EB, Jones JD (1998) Three genes of the Arabidopsis RPP1 complex resistance locus recognize distinct Peronospora parasitica avirulence determinants. Plant Cell 10: 1847–1860
Pubmed: Author and Title

Google Scholar: Author Only Title Only Author and Title

Bowling SA, Guo A, Cao H, Gordon AS, Klessig DF, Dong X (1994) A mutation in Arabidopsis that leads to constitutive expression of systemic acquired resistance. Plant Cell 6: 1845–1857
Pubmed: Author and Title
Google Scholar: Author Only Title Only Author and Title

Cao J, Schneeberger K, Ossowski S, Günther T, Bender S, Fitz J, Koenig D, Lanz C, Stegle O, Lippert C, et al (2011) Whole-genome sequencing of multiple Arabidopsis thaliana populations. Nat Genet 43: 956–963
Pubmed: Author and Title
Google Scholar: Author Only Title Only Author and Title

Chae E, Bomblies K, Kim S-TT, Karelina D, Zaidem M, Ossowski S, Martín-Pizarro C, Laitinen RAEAE, Rowan BAA, Tenenboim H, et al (2014) Species-wide genetic incompatibility analysis identifies immune genes as hot spots of deleterious epistasis. Cell 159: 1341–1351
Pubmed: Author and Title
Google Scholar: Author Only Title Only Author and Title

Chen C, Chen H, Lin Y-S, Shen J-B, Shan J-X, Qi P, Shi M, Zhu M-Z, Huang X-H, Feng Q, et al (2014) A two-locus interaction causes interspecific hybrid weakness in rice. Nat Commun 5: 3357
Pubmed: Author and Title
Google Scholar: Author Only Title Only Author and Title

Clerkx EJM, El-Lithy ME, Vierling E, Ruys GJ, Blankestijn-De Vries H, Groot SPC, Vreugdenhil D, Koornneef M (2004) Analysis of natural allelic variation of Arabidopsis seed germination and seed longevity traits between the accessions Landsberg erecta and Shakdara, using a new recombinant inbred line population. PLANT Physiol 135: 432–443
Pubmed: Author and Title
Google Scholar: Author Only Title Only Author and Title

Coates ME, Beynon JL (2010) Hyaloperonospora arabidopsidis as a pathogen model. Annu Rev Phytopathol 48: 329–345
Pubmed: Author and Title
Google Scholar: Author Only Title Only Author and Title

Coyne JA, Orr HA (2004) Speciation. Sinauer Associates
Pubmed: Author and Title
Google Scholar: Author Only Title Only Author and Title

Coyne JJA (1992) Genetics and speciation. Nature 355: 511–515
Pubmed: Author and Title
Google Scholar: Author Only Title Only Author and Title

Dettman JR, Sirjusingh C, Kohn LM, Anderson JB (2007) Incipient speciation by divergent adaptation and antagonistic epistasis in yeast. Nature 447: 585–588
Pubmed: Author and Title
Google Scholar: Author Only Title Only Author and Title

Dodds PN, Rathjen JP (2010) Plant immunity: towards an integrated view of plant-pathogen interactions. Nat Rev Genet 11: 539–548
Pubmed: Author and Title
Google Scholar: Author Only Title Only Author and Title

Doyle J (1991) DNA protocols for plants. Mol. Tech. Taxon. Springer Berlin Heidelberg, Berlin, Heidelberg, pp 283–293
Pubmed: Author and Title
Google Scholar: Author Only Title Only Author and Title

Earley KW, Haag JR, Pontes O, Opper K, Juehne T, Song K, Pikaard CS (2006) Gateway-compatible vectors for plant functional genomics and proteomics. Plant J 45: 616–629
Pubmed: Author and Title
Google Scholar: Author Only Title Only Author and Title

Falk A, Feys BJ, Frost LN, Jones JD, Daniels MJ, Parker JE (1999) EDS1, an essential component of R gene-mediated disease resistance in Arabidopsis has homology to eukaryotic lipases. Proc Natl Acad Sci U S A 96: 3292–3297
Pubmed: Author and Title
Google Scholar: Author Only Title Only Author and Title

Fauser F, Schiml S, Puchta H (2014) Both CRISPR/Cas-based nucleases and nickases can be used efficiently for genome engineering in Arabidopsis thaliana. Plant J 79: 348–359
Pubmed: Author and Title
Google Scholar: Author Only Title Only Author and Title

Feys BJ, Moisan LJ, Newman MA, Parker JE (2001) Direct interaction between the Arabidopsis disease resistance signaling proteins, EDS1 and PAD4. EMBO J 20: 5400–5411
Pubmed: Author and Title
Google Scholar: Author Only Title Only Author and Title

Feys BJ, Wiermer M, Bhat RA, Moisan LJ, Medina-Escobar N, Neu C, Cabral A, Parker JE (2005) Arabidopsis SENESCENCE-ASSOCIATED GENE101 stabilizes and signals within an ENHANCED DISEASE SUSCEPTIBILITY1 complex in plant innate immunity.

Plant Cell 17: 2601–2613
Pubmed: Author and Title
Google Scholar: Author Only Title Only Author and Title

Flynn KM, Cooper TF, Moore FB-G, Cooper VS (2013) The environment affects epistatic interactions to alter the topology of an empirical fitness landscape. PLoS Genet 9: e1003426
Pubmed: Author and Title
Google Scholar: Author Only Title Only Author and Title

Goritschnig S, Steinbrenner AD, Grunwald DJ, Staskawicz BJ (2016) Structurally distinct Arabidopsis thaliana NLR immune receptors recognize tandem WY domains of an oomycete effector. New Phytol 210: 984–996
Pubmed: Author and Title
Google Scholar: Author Only Title Only Author and Title

Hurwitz BL, Kudrna D, Yu Y, Sebastian A, Zuccolo A, Jackson SA, Ware D, Wing RA, Stein L (2010) Rice structural variation: a comparative analysis of structural variation between rice and three of its closest relatives in the genus Oryza. Plant J 63: 990–1003
Pubmed: Author and Title
Google Scholar: Author Only Title Only Author and Title

Jeuken MJW, Zhang NW, McHale LK, Pelgrom K, den Boer E, Lindhout P, Michelmore RW, Visser RGF, Niks RE (2009) RIN4 causes hybrid necrosis and race-specific resistance in an interspecific lettuce hybrid. Plant Cell 21: 3368–3378
Pubmed: Author and Title
Google Scholar: Author Only Title Only Author and Title

Kang HM, Sul JH, Service SK, Zaitlen NA, Kong S, Freimer NB, Sabatti C, Eskin E (2010) Variance component model to account for sample structure in genome-wide association studies. Nat Genet 42: 348–354
Pubmed: Author and Title
Google Scholar: Author Only Title Only Author and Title

Khan M, Subramaniam R, Desveaux D (2016) Of guards, decoys, baits and traps: pathogen perception in plants by type III effector sensors. Curr Opin Microbiol 29: 49–55
Pubmed: Author and Title
Google Scholar: Author Only Title Only Author and Title

Kopka J, Schauer N, Krueger S, Birkemeyer C, Usadel B, Bergmuller E, Dormann P, Weckwerth W, Gibon Y, Stitt M, et al (2005) GMD@CSB.DB: the Golm Metabolome Database. Bioinformatics 21: 1635–1638
Pubmed: Author and Title
Google Scholar: Author Only Title Only Author and Title

Krasileva K V, Dahlbeck D, Staskawicz BJ (2010) Activation of an Arabidopsis resistance protein is specified by the in planta association of its leucine-rich repeat domain with the cognate oomycete effector. Plant Cell 22: 2444–2458
Pubmed: Author and Title
Google Scholar: Author Only Title Only Author and Title

Krüger J, Thomas CM, Golstein C, Dixon MS, Smoker M, Tang S, Mulder L, Jones JDG (2002) A tomato cysteine protease required for Cf-2-dependent disease resistance and suppression of autonecrosis. Science 296:744-747
Pubmed: Author and Title
Google Scholar: Author Only Title Only Author and Title

McDowell JM, Cuzick A, Can C, Beynon J, Dangl JL, Holub EB (2000) Downy mildew (Peronospora parasitica) resistance genes in Arabidopsis vary in functional requirements for NDR1, EDS1, NPR1 and salicylic acid accumulation. Plant J 22: 523–529
Pubmed: Author and Title
Google Scholar: Author Only Title Only Author and Title

McHale LK, Haun WJ, Xu WW, Bhaskar PB, Anderson JE, Hyten DL, Gerhardt DJ, Jeddeloh JA, Stupar RM (2012) Structural variants in the soybean genome localize to clusters of biotic stress-response genes. Plant Physiol 159: 1295–1308
Pubmed: Author and Title
Google Scholar: Author Only Title Only Author and Title

Meyers BC, Kozik A, Griego A, Kuang H, Michelmore RW (2003) Genome-wide analysis of NBS-LRR-encoding genes in Arabidopsis. Plant Cell 15: 809–34
Pubmed: Author and Title
Google Scholar: Author Only Title Only Author and Title

Muñoz-Amatriaín M, Eichten SR, Wicker T, Richmond TA, Mascher M, Steuernagel B, Scholz U, Ariyadasa R, Spannagl M, Nussbaumer T, et al (2013) Distribution, functional impact, and origin mechanisms of copy number variation in the barley genome. Genome Biol 14: R58
Pubmed: Author and Title
Google Scholar: Author Only Title Only Author and Title

Ono J, Gerstein AC, Otto SP, Walker S, Stewart-Ornstein J, Newman H (2017) Widespread genetic incompatibilities between first-step mutations during parallel adaptation of Saccharomyces cerevisiae to a common environment. PLoS Biol 15: e1002591
Pubmed: Author and Title
Google Scholar: Author Only Title Only Author and Title

van Ooijen G, Mayr G, Kasiem MM a, Albrecht M, Cornelissen BJC, Takken FLW (2008) Structure-function analysis of the NB-ARC domain of plant disease resistance proteins. J Exp Bot 59: 1383–1397
Pubmed: Author and Title
Google Scholar: Author Only Title Only Author and Title

Rehmany AP, Gordon A, Rose LE, Allen RL, Armstrong MR, Whisson SC, Kamoun S, Tyler BM, Birch PRJ, Beynon JL (2005) Differential recognition of highly divergent downy mildew avirulence gene alleles by RPP1 resistance genes from two Arabidopsis lines. Plant Cell 17: 1839–1850
Pubmed: Author and Title
Google Scholar: Author Only Title Only Author and Title

Schreiber KJ, Bentham A, Williams SJ, Kobe B, Staskawicz BJ, Meng E (2016) Multiple domain associations within the Arabidopsis immune receptor RPP1 regulate the activation of programmed cell death. PLoS Pathog 12: e1005769
Pubmed: Author and Title
Google Scholar: Author Only Title Only Author and Title

Seren Ü, Vilhjálmsson BJ, Horton MW, Meng D, Forai P, Huang YS, Long Q, Segura V, Nordborg M (2012) GWAPP: a web application for genome-wide association mapping in Arabidopsis. Plant Cell 24: 4793–4805
Pubmed: Author and Title
Google Scholar: Author Only Title Only Author and Title

Sherlock G, Petrov DA, Levy S, Agarwala A, Chang J, Ebel E (2017) Seeking goldilocks during evolution of drug resistance. PLoS Biol 15: e2001872
Pubmed: Author and Title
Google Scholar: Author Only Title Only Author and Title

Sicard A, Kappel C, Josephs EB, Lee YW, Marona C, Stinchcombe JR, Wright SI, Lenhard M (2015) Divergent sorting of a balanced ancestral polymorphism underlies the establishment of gene-flow barriers in Capsella. Nat Commun 6: 7960
Pubmed: Author and Title
Google Scholar: Author Only Title Only Author and Title

Smith AM, Zeeman SC (2006) Quantification of starch in plant tissues. Nat Protoc 1: 1342–1345
Pubmed: Author and Title
Google Scholar: Author Only Title Only Author and Title

Sohn KH, Lei R, Nemri A, Jones JDG (2007) The downy mildew effector proteins ATR1 and ATR13 promote disease susceptibility in Arabidopsis thaliana. Plant Cell 19: 4077–4090
Pubmed: Author and Title
Google Scholar: Author Only Title Only Author and Title

Steinbrenner AD, Goritschnig S, Staskawicz BJ (2015) Recognition and activation domains contribute to allele-specific responses of an Arabidopsis NLR receptor to an oomycete effector protein. PLoS Pathog 11: e1004665
Pubmed: Author and Title
Google Scholar: Author Only Title Only Author and Title

Stuttmann J, Peine N, Garcia A V., Wagner C, Choudhury SR, Wang Y, Velikkakam James G, Griebel T, Alcázar R, Tsuda K, et al (2016) Arabidopsis thaliana DM2h (R8) within the Landsberg RPP1-like resistance locus underlies three different cases of EDS1- conditioned autoimmunity. PLoS Genet 12: e1005990
Pubmed: Author and Title
Google Scholar: Author Only Title Only Author and Title

Sukarta OCA, Slootweg EJ, Goverse A (2016) Structure-informed insights for NLR functioning in plant immunity. Semin Cell Dev Biol 56: 134–149
Pubmed: Author and Title
Google Scholar: Author Only Title Only Author and Title

Swiderski MR, Birker D, Jones JDG (2009) The TIR domain of TIR-NB-LRR resistance proteins is a signaling domain involved in cell death induction. Mol Plant-Microbe Interact 22: 157–165
Pubmed: Author and Title
Google Scholar: Author Only Title Only Author and Title

Takken FLW, Goverse A (2012) How to build a pathogen detector: structural basis of NB-LRR function. Curr Opin Plant Biol 15: 375–384
Pubmed: Author and Title
Google Scholar: Author Only Title Only Author and Title

Tauzin AS, Giardina T (2014) Sucrose and invertases, a part of the plant defense response to the biotic stresses. Front Plant Sci 5: 293
Pubmed: Author and Title
Google Scholar: Author Only Title Only Author and Title

Wildermuth MC, Dewdney J, Wu G, Ausubel FM (2001) Isochorismate synthase is required to synthesize salicylic acid for plant defence. Nature 414: 562–565
Pubmed: Author and Title
Google Scholar: Author Only Title Only Author and Title

Williams SJ, Sohn KH, Wan L, Bernoux M, Sarris PF, Segonzac C, Ve T, Ma Y, Saucet SB, Ericsson DJ, et al (2014) Structural basis for

assembly and function of a heterodimeric plant immune receptor. Science 344: 299–303
Pubmed: Author and Title
Google Scholar: Author Only Title Only Author and Title

Xu X, Liu X, Ge S, Jensen JD, Hu F, Li X, Dong Y, Gutenkunst RN, Fang L, Huang L, et al (2011) Resequencing 50 accessions of cultivated and wild rice yields markers for identifying agronomically important genes. Nat Biotechnol 30: 105–111
Pubmed: Author and Title
Google Scholar: Author Only Title Only Author and Title

Yamamoto E, Takashi T, Morinaka Y, Lin S, Wu J, Matsumoto T, Kitano H, Matsuoka M, Ashikari M (2010) Gain of deleterious function causes an autoimmune response and Bateson-Dobzhansky-Muller incompatibility in rice. Mol Genet Genomics 283: 305–315
Pubmed: Author and Title
Google Scholar: Author Only Title Only Author and Title

Yuan J, He SY (1996) The Pseudomonas syringae Hrp regulation and secretion system controls the production and secretion of multiple extracellular proteins. J Bacteriol 178: 6399–6402
Pubmed: Author and Title
Google Scholar: Author Only Title Only Author and Title

Zarza X, Atanasov KE, Marco F, Arbona V, Carrasco P, Kopka J, Fotopoulos V, Munnik T, Gómez-Cadenas A, Tiburcio AF, et al (2017) Polyamine oxidase 5 loss-of-function mutations in Arabidopsis thaliana trigger metabolic and transcriptional reprogramming and promote salt stress tolerance. Plant Cell Environ 40: 527–542
Pubmed: Author and Title
Google Scholar: Author Only Title Only Author and Title

Zhang X, Bernoux M, Bentham AR, Newman TE, Ve T, Casey LW, Raaymakers TM, Hu J, Croll TI, Schreiber KJ, et al (2017) Multiple functional self-association interfaces in plant TIR domains. Proc Natl Acad Sci 114: E2046–E2052
Pubmed: Author and Title
Google Scholar: Author Only Title Only Author and Title

Zhang Z, Ersoz E, Lai C-Q, Todhunter RJ, Tiwari HK, Gore MA, Bradbury PJ, Yu J, Arnett DK, Ordovas JM, et al (2010) Mixed linear model approach adapted for genome-wide association studies. Nat Genet 42: 355–360
Pubmed: Author and Title
Google Scholar: Author Only Title Only Author and Title